NAVAL POSTGRADUATE SCHOOL

MONTEREY, CALIFORNIA

THESIS

FUNCTIONALLY GRADED ALUMINUM METAL MATRIX COMPOSITE COLD SPRAY COATINGS ON ALUMINUM 7075 SUBSTRATE

by

Nicolas W. Twisselman

June 2023

Thesis Advisor: Troy Ansell
Second Reader: Young W. Kwon

THIS PAGE INTENTIONALLY LEFT BLANK

REPORT DOCUMENTATION PAGE			*Form Approved OMB No. 0704-0188*

1. AGENCY USE ONLY *(Leave blank)*	**2. REPORT DATE** June 2023	**3. REPORT TYPE AND DATES COVERED** Master's thesis

4. TITLE AND SUBTITLE FUNCTIONALLY GRADED ALUMINUM METAL MATRIX COMPOSITE COLD SPRAY COATINGS ON ALUMINUM 7075 SUBSTRATE	**5. FUNDING NUMBERS** RMKT1
6. AUTHOR(S) Nicolas W. Twisselman	
7. PERFORMING ORGANIZATION NAME(S) AND ADDRESS(ES) Naval Postgraduate School Monterey, CA 93943-5000	**8. PERFORMING ORGANIZATION REPORT NUMBER**
9. SPONSORING / MONITORING AGENCY NAME(S) AND ADDRESS(ES) Office Of Naval Research, Young Investigator Program. Arlington, VA, 22217	**10. SPONSORING / MONITORING AGENCY REPORT NUMBER**

11. SUPPLEMENTARY NOTES The views expressed in this thesis are those of the author and do not reflect the official policy or position of the Department of Defense or the U.S. Government.

12a. DISTRIBUTION / AVAILABILITY STATEMENT Approved for public release. Distribution is unlimited.	**12b. DISTRIBUTION CODE** A

13. ABSTRACT (maximum 200 words)

Aluminum alloys have widespread use in the aerospace and maritime industries due to their high specific strength, good corrosion resistance, and low cost. Gas dynamic cold spray, cold spray for short, is a thermal spray technique that is used for in-field repair of metallic surfaces to include aluminum. To improve the wear resistance of aluminum, the metal must be reinforced with a filler. Additionally, to prevent delamination issues with cold sprayed coatings, a compositionally graded coating is required. To date, there has not been a study on the cold spray of compositionally graded, dual-reinforced aluminum metal matrix composites (Al-MMC). Al reinforced with aluminum oxide (Al2O3) and boron nitride nanotubes (BNNT) were cold-sprayed onto aircraft-grade aluminum (Al-7075) alloy. High energy ball milling was used to create coating compositions of 10, 20, and 30 vol.% Al2O3, 2 vol.% BNNTs, as well as 1 vol.% BNNT with 10 vol.% Al2O3. The different coating compositions were then graded over one another by means of cold spray and their subsequent properties of adhesion strength and wear resistance were studied. Results from these tests were also qualitatively evaluated using optical and scanning electron microscopy, as well as optical profilometry. All four graded coating compositions experienced equal or increased adhesion strength, while failing cohesively, leaving the base cold spray composition intact, i.e., still adhered to the substrate.

14. SUBJECT TERMS aluminum, aluminum oxide, alumina, ball-to-powder ratio, boron carbide, boron nitride nanoplatelet, energy-dispersive X-ray spectroscopy, high energy ball milling, metal matrix composite, micro-boron carbide, scanning electron microscope	**15. NUMBER OF PAGES** 105
	16. PRICE CODE

17. SECURITY CLASSIFICATION OF REPORT	**18. SECURITY CLASSIFICATION OF THIS PAGE**	**19. SECURITY CLASSIFICATION OF ABSTRACT**	**20. LIMITATION OF ABSTRACT**
Unclassified	Unclassified	Unclassified	UU

NSN 7540-01-280-5500

Standard Form 298 (Rev. 2-89)
Prescribed by ANSI Std. 239-18

THIS PAGE INTENTIONALLY LEFT BLANK

Approved for public release. Distribution is unlimited.

FUNCTIONALLY GRADED ALUMINUM METAL MATRIX COMPOSITE COLD SPRAY COATINGS ON ALUMINUM 7075 SUBSTRATE

Nicolas W. Twisselman
Lieutenant Commander, United States Navy
BS, Oregon State University, 2011

Submitted in partial fulfillment of the
requirements for the degree of

MASTER OF SCIENCE IN MECHANICAL ENGINEERING

from the

NAVAL POSTGRADUATE SCHOOL
June 2023

Approved by: Troy Ansell
Advisor

Young W. Kwon
Second Reader

Brian S. Bingham
Chair, Department of Mechanical and Aerospace Engineering

THIS PAGE INTENTIONALLY LEFT BLANK

ABSTRACT

Aluminum alloys have widespread use in the aerospace and maritime industries due to their high specific strength, good corrosion resistance, and low cost. Gas dynamic cold spray, cold spray for short, is a thermal spray technique that is used for in-field repair of metallic surfaces to include aluminum. To improve the wear resistance of aluminum, the metal must be reinforced with a filler. Additionally, to prevent delamination issues with cold sprayed coatings, a compositionally graded coating is required. To date, there has not been a study on the cold spray of compositionally graded, dual-reinforced aluminum metal matrix composites (Al-MMC). Al reinforced with aluminum oxide (Al2O3) and boron nitride nanotubes (BNNT) were cold-sprayed onto aircraft-grade aluminum (Al-7075) alloy. High energy ball milling was used to create coating compositions of 10, 20, and 30 vol.% Al2O3, 2 vol.% BNNTs, as well as 1 vol.% BNNT with 10 vol.% Al2O3. The different coating compositions were then graded over one another by means of cold spray and their subsequent properties of adhesion strength and wear resistance were studied. Results from these tests were also qualitatively evaluated using optical and scanning electron microscopy, as well as optical profilometry. All four graded coating compositions experienced equal or increased adhesion strength, while failing cohesively, leaving the base cold spray composition intact, i.e., still adhered to the substrate.

THIS PAGE INTENTIONALLY LEFT BLANK

TABLE OF CONTENTS

I. MOTIVATION AND OBJECTIVES 1

A. MOTIVATION 1
B. OBJECTIVES 1

II. BACKGROUND 3

A. WHAT IS COLD SPRAY 3
B. WEAR RESISTANCE 7
C. ADHESION STRENGTH 8
D. ALUMINUM METAL MATRIX COMPOSITES 9
E. BORON NITRIDE NANOTUBES 10
F. ALUMINA 12
G. POWDER PROCESSING 14

III. EXPERIMENTAL METHODS AND PROCEDURES 17

A. MATERIALS SELECTION 17
B. METAL MATRIX COMPOSITE 19
C. ALUMINUM 7075 SUBSTRATE 22
D. HIGH ENERGY BALL MILLING 22
E. COLD SPRAYING 24
F. SAMPLE PREPARATION AND STORAGE 27
G. MECHANICAL TESTING 30
1. Adhesion 30
2. Wear Testing 32
H. CHARACTERIZATION 33

IV. RESULTS AND DISCUSSION 37

A. POWDER COMPOSITION AND CHARACTERIZATION 37
1. Al-7075 and BNNT Powder 37
2. Al-7075 and Alumina Powder 40
3. Al-7075, Alumina, and BNNT Powder 41
B. COLD SPRAY SAMPLE CHARACTERIZATION 46
1. Visual Inspection 46
2. Optical Microscopy 47
3. SEM Microstructural Characterization 48
4. SEM Top-Down Imagery of Top Layer Compositions of Cold Spray Coatings 59

C. ADHESION 61
D. WEAR 70

V. CONCLUSION 77
A. SUMMARY 77
B. RECOMMENDATIONS FOR FUTURE WORKS 77

LIST OF REFERENCES 79

INITIAL DISTRIBUTION LIST 85

LIST OF FIGURES

Figure 1. Comparison of thermal spray processes. Source: [7]..... 4

Figure 2. Typical cold spray process. Source: [9]..... 4

Figure 3. Cold spray use of de Laval nozzle type. Source: [13]. 6

Figure 4. Scopus Search Results regarding BNNTs: (A) 2000-2019 Annual Peer Reviewed Publications CNT and BNNT (BNNT columns are hardly visible). (B) Cumulative number of CNT and BNNT publications (BNNT is blue line following horizontal axis). Source: [25]..... 11

Figure 5. Structure of CNT (left) and BNNT (right). Source: [26]..... 12

Figure 6. Measured and estimated hardness of coatings vs. coating alumina contents. Source: [30]. 14

Figure 7. HEBM effects on 316L stainless steel powders. Source [31]..... 16

Figure 8. Al-7075 powder as received from manufacturer 1kX magnification. 18

Figure 9. Al-7075 Powder as received from the manufacturer 10kX magnification. 18

Figure 10. Alumina as received from manufacturer..... 19

Figure 11. Alumina particles adhering to Al-7075 post HEBM. 20

Figure 12. TEM image of a BNNT, as received from the manufacturer. Source: [3]..... 21

Figure 13. SEM image of BNNT agglomerations, as received from manufacturer 21

Figure 14. Top-down view of cold spray coatings..... 26

Figure 15. Struers Secotom-20..... 28

Figure 16. Struers CitoPress-10..... 28

Figure 17. Unpolished puck 29

Figure 18. Polished puck..... 29

Figure 19. Nanovea T50 tribometer 33

Figure 20. Zeiss Neon 40 SEM. 35

Figure 21. Helios 5 UX SEM. 35

Figure 22. Al-7075 and BNNT post HEBM 38

Figure 23. Agglomeration of BNNTs within Al-7075 post HEBM..... 39

Figure 24. Individual BNNT located on surface of Al-7075 particle 40

Figure 25. SEM Image of Al-7075 with 10 vol.% alumina 41

Figure 26. Al-7075, BNNT, and Alumina powder post HEBM 42

Figure 27. Two Al-7075 particles bridged with alumina 43

Figure 28. Alumina bridging several Al-7075 particles as seen circled in red 43

Figure 29. Surface adhesion of alumina on Al-7075 particle..... 44

Figure 30. BNNT location on Al-7075 particle 45

Figure 31. Individual BNNT located on Al-7075 particle as seen in Figure 30 45

Figure 32. Cold spray compositions. Left to right: 10vol.% Al2O3 with Al-7075, 20vol.% Al2O3 with Al-7075, 30vol.% Al2O3 with Al-7075, 30vol.% Al2O3 with Al-7075 (middle coating layer composed of 1 vol.% BNNT, 10 vol.% Al2O3. 89 vol.% Al-7075. Note, all coating base layers are 2 vol.% BNNT with Al-7075 47

Figure 33. Optical microscope images of all four compositions. Starting top left clockwise: 10vol.% Al2O3 with Al-7075, 20vol.% Al2O3 with Al-7075, 30vol.% Al2O3 with Al-7075, 30vol.% Al2O3 with Al-7075 (middle coating layer composed of 1 vol.% BNNT, 10 vol.% Al2O3. 89 vol.% Al-7075. Note, all coating base layers are 2 vol.% BNNT with Al-7075 48

Figure 34. SEM thickness measurements of AL-7075 with 10 vol.% alumina 50

Figure 35. SEM image of splat boundaries found within the coating..... 51

Figure 36. SEM image of coating at lower magnification 52

Figure 37. SEM image of Al-7075/BNNT control coating..... 54

Figure 38. BNNT base layer, as seen in red, of coating 3..... 54

Figure 39. Compositional layering of coating 4 55

Figure 40. SEM image of alumina at coating interface of coating 1 56

Figure 41. SEM image of alumina within splat boundary interface with individual alumina particle bridging splat boundary of coating 3 57

Figure 42. SEM image of individual BNNT located in coating 1 58

Figure 43. SEM image of possible BNNTs bridging splat boundary of coating 4, as circled in red (350kX magnification) 58

Figure 44. Top-down SEM images of top layer compositions of cold spray coatings 60

Figure 45. Top-down SEM image of impact crater on coating 1 61

Figure 46. Adhesion test post failure for coating 3 62

Figure 47. Adhesion results 64

Figure 48. Top-down SEM image of coating 1 in failure zone 66

Figure 49. Top-down SEM of coating 2 in failure zone 67

Figure 50. Top-down SEM image of BNNTs located in coating 2 68

Figure 51. Top-down SEM image within adhesion failure zone of coating 4 69

Figure 52. Average mass loss (grams) during wear testing 71

Figure 53. Coefficient of friction for coatings during wear testing. (Clockwise from top left: graded coating 1, graded coating 2, graded coating 4, graded coating 3) 72

Figure 54. Encoder depth during wear testing. (Clockwise from top left: graded coating 1, graded coating 2, graded coating 4, graded coating 3) 73

Figure 55. Optical profilometry scan for graded coating 2. 75

Figure 56. Optical profilometry depth reading for graded coating 4. 75

THIS PAGE INTENTIONALLY LEFT BLANK

LIST OF TABLES

Table 1. Al-7075 alloy. Elemental composition in wt%. Source: [39]. 22

Table 2. Cold spray coating compositions 23

Table 3. Powder densities 23

Table 4. HEBM parameters for Al-7075 w/ 10 vol.% alumina 24

Table 5. Final spraying parameters 26

Table 6. Polishing parameters 27

Table 7. Adhesion coating sample compositions 31

Table 8. Adhesion test parameters 31

Table 9. Wear testing parameters 33

Table 10. Average coating thickness 49

Table 11. Coating compositions 53

Table 12. Graded cold spray compositions and adhesion strength 62

Table 13. Control cold spray compositions and adhesion strength 63

Table 14. Average wear depths and specific wear rates 74

THIS PAGE INTENTIONALLY LEFT BLANK

LIST OF ACRONYMS AND ABBREVIATIONS

Al	aluminum
Al-7075	aluminum 7075 alloy
Al_2O_3	alumina, aluminum oxide
AM	additive manufacturing
ASTM	American Society for Testing and Materials
BNNB	boron nitride nanobarb
BNNT	boron nitride nanotube
BPR	ball to powder ratio
CMC	ceramic matrix composite
CNT	carbon nanotube
CVD	chemical vapor deposition
DOD	Department of Defense
He	helium
HEBM	high energy ball mill
HVOF	high velocity oxygen fuel
HTP	high temperature and pressure
IAW	in accordance with
MMC	metal matric composite
nD	nano diamond
RPM	revolutions per minute
SBM	solution ball milling
SiC	silicon carbide
SEM	scanning electron microscope
SS	stainless steel
TEM	transmission electron microscope
Vol.%	volume percentage
Wt.%	weight percentage

THIS PAGE INTENTIONALLY LEFT BLANK

ACKNOWLEDGMENTS

I would like to thank my late thesis advisor, Dr. Andy Nieto. His guidance and mentorship proved invaluable during our time together at NPS.

I would also like to thank Dr. Troy Ansell. Dr. Ansell was not only a mentor, but provided the guidance and experience needed to be successful here at NPS, especially during trying times. No matter the issue, Dr. Ansell was always unflappable, continuously steering the course to the right heading.

Lastly, I would like to thank my wife, Mary. Without her support and patience none of this would have been possible.

THIS PAGE INTENTIONALLY LEFT BLANK

I. MOTIVATION AND OBJECTIVES

A. MOTIVATION

Up until this point there have been nearly no studies on functionally graded cold spray processes incorporating boron nitride nanotubes (BNNT) and alumina (Al_2O_3) incorporating widely used 7075 aluminums, which is commonly used in the aeronautical and marine industries [1]. The goal of this thesis is to investigate the potential impacts graded cold sprayed layers will have on the adhesion and wear resistance properties of an aluminum substrate.

The Unites States Navy shipyards have been incorporating the cold spray process into their maintenance approach for several years due the flexibility it grants from its application process [2]. Other intrinsic properties make the use of cold spray favorable by many maintenance providers. Specifically, its ability to be applied at much lower temperatures as opposed to other thermal spray techniques like plasma spray, as well as proven increases in corrosion and wear resistance over unsprayed surfaces [2]. The primary operating area for the United States Navy is the maritime domain, which is an environment that interacts harshly with all platforms, making corrosion and wear related issues a top concern. Cold spray is a technique that could mitigate these issues in a tangible matter. The lightweight properties coupled with its ease of application has the potential to extend operating life of Naval platforms and equipment while reducing costs of both scheduled and unscheduled maintenance.

B. OBJECTIVES

The aim of the work is to investigate the mechanical properties associated with adhesion and wear resistance to a 7075-aluminum (Al-7075) substrate sprayed with functionally graded layers of BNNTs, alumina, and Al-7075 powder. The use of BNNTs have primarily been used in various aspects of manufacturing and industry and have only recently been investigated for cold spray applications [3]. Tauber showed that BNNTs, when incorporated into an aluminum metal matrix composites, produced cold spray coatings that provided strong adhesion to a magnesium substrate [3]. Coupling the adhesive

strength that BNNTs could potentially provide with graded metal matrix composite layers consisting of a hard ceramic phase, such as alumina, would not only be novel in nature but have potential in the growing application of cold spray technology and material science. Alumina has a proven history of increasing mechanical properties such as wear resistance in Al and other metals [4].

This study will look at the adhesion strength and wear resistance of varying volume percentages (vol.%) of alumina in the MMC graded over a basecoat of 2 vol.% BNNTs with Al-7075. To date, there is not published literature on the effects of a graded cold spray coating incorporating BNNTs and alumina with use on an Al-7075 substrate. This thesis intends not only to investigate the mechanical properties but also lay the foundation for future work in the application and use of BNNTs and graded alumina cold spray coating. All cold sprayed coatings and their corresponding microstructures were investigated and characterized using optical and scanning electron microscopes (SEM). The mechanical properties of adhesion and wear resistance were preformed through laboratory tests and further analyzed using characterization techniques in the SEM.

II. BACKGROUND

A. WHAT IS COLD SPRAY

Gas dynamic cold spray (cold spray) is a process in which powder is deposited onto a substrate at high enough velocities that the powder will mechanically bond with the substrate. What separates cold spray from similar deposition techniques, such as plasma spray and high velocity oxygen fuel (HVOF), is that cold spray maintains temperatures below the melting point of the metal powders being deposited. Methods such as HVOF will effectively melt the powders as they are being deposited and adhesion to the substrate occurs after the solidification of the metal powders. Cold spray achieves adhesion to the substrate by accelerating the metal powder particles to a minimal critical velocity, usually between 300-1200 m/s [5] and upon impact to the substrate the powder undergoes solid state bonding to the substrate. Powder deposition of cold spray is done via a carrier gas, usually helium or nitrogen, and heated to temperatures usually ranging between 300-500 °C [5], whereafter the feed powder is introduced and then passed through a convergent-divergent de Laval nozzle where critical velocities of the particle are reached before impact and subsequent adhesion to the substrate. When compared to other methods of material deposition (see Figure 1), cold spray coatings maintain temperatures lower than the melting temperature of the deposited material which enables the cold sprayed coatings to maintain many of the characteristics of the powder that was deposited. Some of these material characteristics include high corrosion resistance, high density, low porosity, high bond strength, no grain growth, high hardness, no phase change [6], and the use of nano-size reinforcements [7].

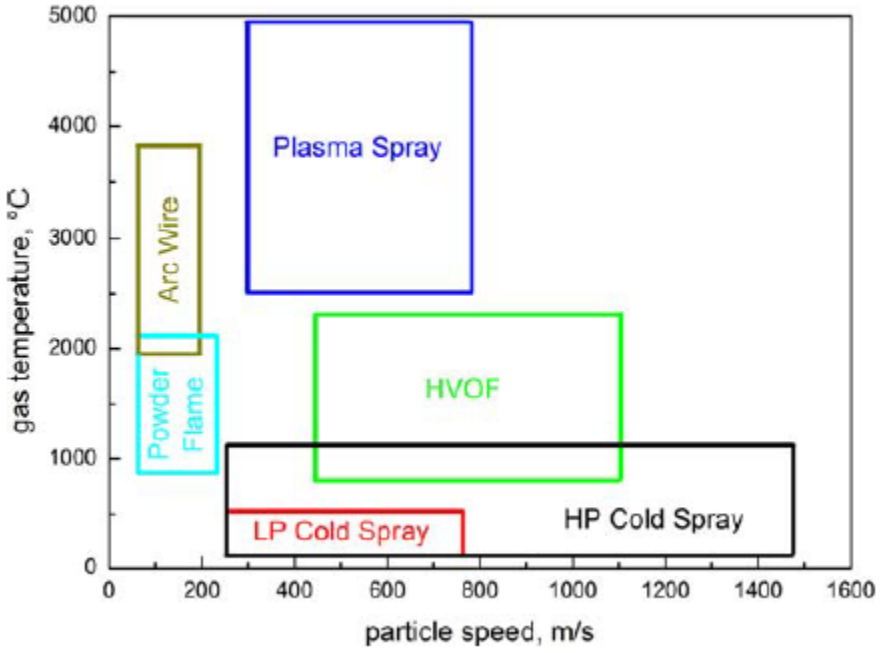

Figure 1. Comparison of thermal spray processes. Source: [7].

The operating equipment for cold spraying remains fundamentally the same between various manufacturers. The typical setup requires compressed gas (usually helium or nitrogen [8]), an operations control station, a powder feeder (typically in line with the operations control station), and electronic heater, and a de Laval nozzle. See Figure 2.

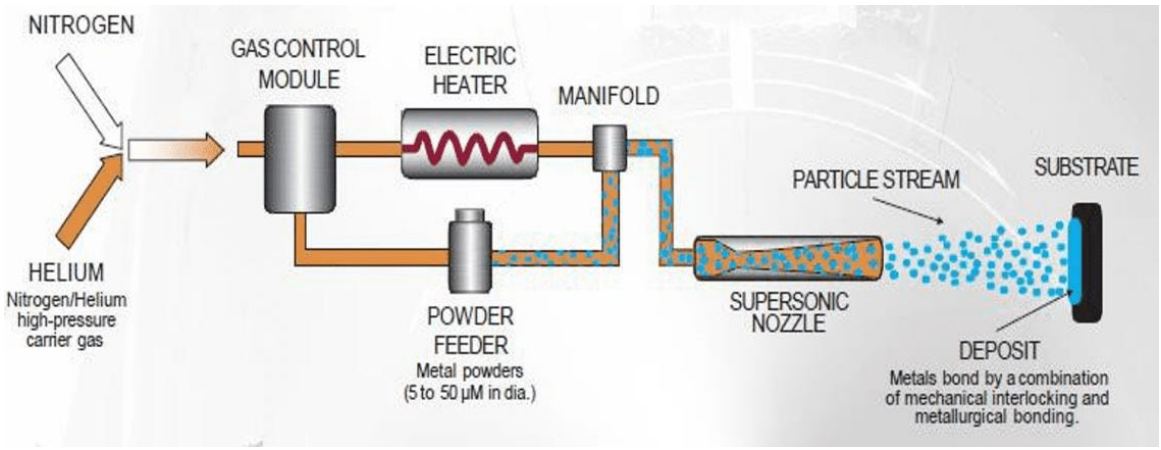

Figure 2. Typical cold spray process. Source: [9].

One of the most crucial elements to the cold spraying process is the velocity that the powder particles reach before impact with the substrate. There are several factors that contribute to the requirement for the particle's velocity. Mainly, the material properties of the powder being sprayed, pressure, gas type, size and shape of the powder particles, distance from nozzle to substrate, and nozzle design are among a few parameters [10]. The velocity that is required in order to bond the sprayed powder to the substrate is known as the critical velocity [8].

The first step in obtaining critical velocity during the cold spray process is from using a heated gas as the propellant for the powder. The heater raises the temperature of the injected gas, and subsequently raises the temperature of the powder once the powder is fed into the system. By increasing the temperature and pressure of the gas, the particle velocity exiting the nozzle will also increase. The two most common gases used are helium and nitrogen [8]. Nitrogen (N_2) is generally preferred due to its low cost and wider availability. However, helium (He) is used when trying to improve the adhesion and coating porosity when spraying onto high-grade alloys. Helium has more suitable thermal properties that consequently allows the gas to be brought up to higher Mach numbers which in turn increases the particle velocities upon impact. Additionally, He has a higher specific heat ratio and specific gas constant when compared to N_2 [8].

The last step to achieve critical velocity during the cold spray process is the use of a de Laval nozzle. A de Laval nozzle is a converging-diverging type nozzle which is used to accelerate the fluid (powder and gas) to supersonic speeds by converting thermal energy to kinetic energy via a difference in pressure [11]. The convergence section of the nozzle has fluid (powder and gas) moving at subsonic speeds, whereas the divergence section the gas is allowed to expand and the velocity of the fluid (powder) is realized at supersonic speeds [12]. Figure 3 shows the flow path of powders through a de Laval type nozzle deposition site on the substrate.

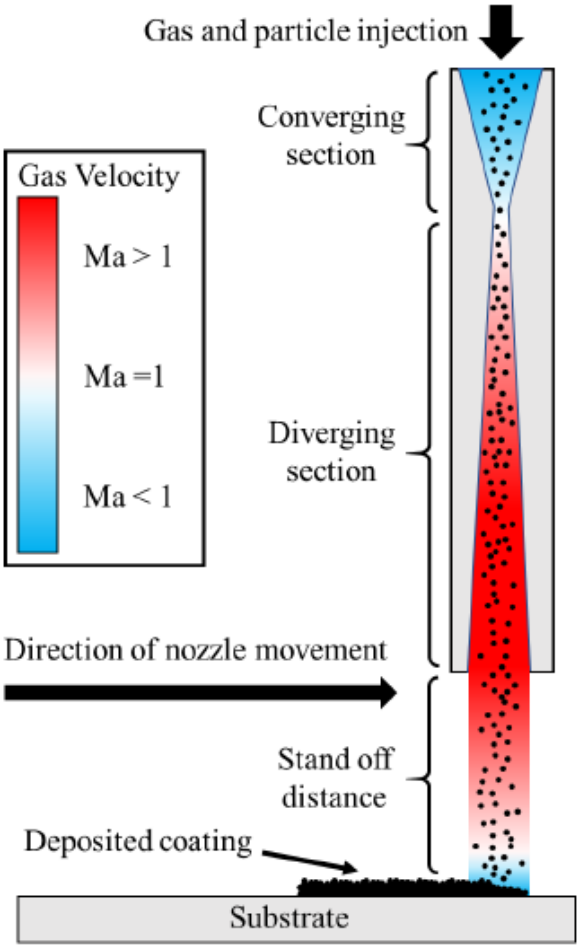

Figure 3. Cold spray use of de Laval nozzle type. Source: [13].

Once the powder has reached its critical velocity and exited the de Laval nozzle, the powder will impact the substrate and plastically deform into flattened out areas known as splats, this is where the boning of the coating and the substrate occurs. The mechanisms of bonding during the cold spray process are not fully understood, as there are several ways that the powder particles can bond to the substrate. Likely, adhesion occurs through a combination of several different mechanisms. One of these mechanisms of potential bonding is that the particles sustain damage to their thin surface layer (such as an oxide layer) and because of such high local pressures, bonding occurs [14]. Another mechanism of potential bonding is plastic deformation causes interparticle cohesion for ductile materials (such as metals) while fragmentation and self-consolidation is achieved from the

stacking of the deposited particles (such as ceramics) [5]. Whichever mechanism is correct, bonding mainly occurs due to metallurgical bonding, mechanical anchoring, interfacial cohesion, or mechanical interlocking [5].

There is one thing that allows cold spray to stand alone from other material deposition processes and that is its low application temperatures. The avoidance of melting of the coating material and solidification of the melt at the substrate, gives cold spray an advantage over other techniques that have been historically employed.

B. WEAR RESISTANCE

Wear of a material is most commonly defined as the gradual modification in material mass or volume with the association of the loss of material in the form of loose debris or the displacement of material when considering wear of a ductile specimen [15]. In either of these situations, plastic deformation occurs. There are numerous types of wear that occur, but the tribological focus, when considering cold spray, is sliding wear and abrasive wear. Sliding wear can be viewed as more of a volume displacement with minimal mass loss, whereas abrasive wear has more mass loss in comparison [15]. It is common when the metal matrix composite (MMC) of a cold spray coating has ceramic particles that sliding wear can transition to abrasive wear due to the ceramic particles breaking free and contributing to grinding of the surface.

There are numerous ways to test wear. Tests range from pin-on-disk devices to intricate devices where users can input variable load and speed cycles [15]. Another aspect of wear testing is that many of the variables involved with the tests may affect the others. This is why it is important when conducting wear tests on materials that the user input conditions that might be most commonly seen in the operating environment for the specific material [15]. There have also been several equations that have been developed to quantify wear, specifically delamination wear, adhesion wear, oxidation wear, fatigue wear, among others [15]. However, these equations result in linear approximations and do not take into account the full spectrum of outcomes possible in wear [15]. Specifically when talking about sliding and abrasive wear, effects such as loading, surface deformation, plastic

strains, and cracking cannot be characterized by the use of linear equations and must be analyzed but other investigative techniques [15].

When considering wear resistance, the ability to resist plastic deformation will ultimately result in the material having a higher resistance to wear. Higher wear resistance typically means higher hardness of the material. When considering cold spray and its applications, it is important to strive for a coating that exhibits hardness and other mechanical properties within a range of acceptable values for the application the material is designed for.

C. ADHESION STRENGTH

Of all the properties associated with cold spray, adhesion is arguably the most important. Adhesion between the deposited powder and the substrate dictates how well the coating will conform to its intended uses. Adhesion of a cold spray coating is influenced by many factors. The primary factor that affects the adhesion of the cold spray coating is the velocity of the particles as they impact the substrate. This velocity is influenced by several factors, specifically temperature of the carrier gas, the corresponding temperature of the powder, the size and shape of the particles, and distribution of the particles within the powder [5]. As previously discussed, the carrier gas plays a role when it comes to the particle's critical velocity. The particle will adhere to the substrate only if deformed upon impact, and the minimum speed required for this deformation is known as the critical velocity [16]. As particles collide and consequently deform on the substrate they are formed into splats. These splats can be characterized by how severely deformed the particles becomes. This deformation when compared to the critical velocity is referred to by Assadi et al. as the flattening ratio [17], defined in Equation 1 below where FR denotes the flattening ratio, h_p denotes the height of the splat particle flattened during impact, and d_p denotes the particle diameter [17].

$$FR = 1 - \frac{h_p}{d_p} \tag{1}$$

The critical velocity and flattening ratio are influenced by the temperature of the gas moving the particles. As the temperature of the gas increases, the ductility of the particles is also increased which directly increases the flattening ratio, which in turn would reduce the required critical velocity value [17]. The more severe the splat the more likely the coating is exhibit decreased porosity, greater amounts of adhered area, and higher values of cohesive strength [17].

D. ALUMINUM METAL MATRIX COMPOSITES

The diversity of cold spray coatings is very extensive. Many times, the desired coating may be a single element, such as pure aluminum, other times an alloy may be desired, such as aluminum 7075. In recent years, the use of various combinations of elements, alloys, and ceramics has seen growth in usage and application when applied to cold spray. Often the operational use for the cold spray coating will determine the type of coating that is applied. For example, if an aluminum coating is going to be in an environment where wear resistance is an important factor, it might be beneficial to include a certain volume percentage of ceramics with an aluminum alloy powder that will used for the cold spray coating. These combinations are commonly referred to as metal matrix composites (MMC).

MMC coatings have proven to be very attractive in industry due to their unique combination of hardness, toughness, and strength. These reinforcement particles which contribute to the increased hardness are usually sourced from various ceramics and then distributed within the ductile matrix [18]. Although many metals can be used in an MMC, aluminum (Al) and its alloys have seen the most widespread use for matrix materials [19]. The properties of an Al based MMC can be customized by choosing the appropriate Al-alloy with a reinforcement particle that complements the enhancement of desired mechanical properties. Aluminum, which already possesses the properties of high strength and light weight, can be made even stronger with the inclusion of even lighter and stronger ceramics. This could even be enhanced further if certain nanoparticles are added to the Al-MMC. Norrell et al. [20] reinforced aluminum coatings with nano boron carbide (nB_4C) and boron nitride nanoplatelets (BNNP) and found that when these Al-MMCs were applied

to an aluminum alloy AA7075 substrate the hardness of improved nearly 12%. However, it was observed that the nB_4C and BNNP reinforced coatings experienced significant pitting and corrosion after exposure to a simulated marine environment [20]. The presence of the nanoparticles in the Norrell experiments interrupted the formation of the passivation layer, Al_2O_3, which forms a protective barrier better suited for resistance to corrosion. In a separate study, Irissou et al. investigated the effect alumina had when blended with Al-MMCs at varying concentrations [21]. It was concluded that volume fractions around 30% alumina contributed to an increase in hardness with no detrimental effect on the corrosion protection of the substrate. To date there has been no studies on the effect of grading cold spray coating layers with different reinforcements on the Al-MMC, as well as differing concentrations of the reinforcing cermet in the graded layers of the coatings.

E. BORON NITRIDE NANOTUBES

In recent years there has been an increased interest in carbon nanotube-metal matrix composites (CNT-MMCs) due to their load bearing capability when aiding in the strengthening of light-weight aluminum [22]. However, one of the drawbacks of CNTs is their low oxidation resistance at increased temperatures [22]. To combat the inadequacies of CNTs, boron nitride nanotubes (BNNTs) have been employed as the more advantageous structural reinforcement due to their impressive mechanical properties [22]. BNNTs have almost analogous mechanical properties as CNTs with a >1 TPa elastic modulus (the highest for lightweight nano materials) and approximately 61 GPa strength but have shown to have better chemical and thermal indolence when compared to CNTs [22]. The introduction of BNNTs as an Al-MMC reinforcement would mean that the composite would not be vulnerable to oxidation at high temperatures. BNNTs have also shown an ability to be a very effective radiation shield due to their high neutron absorption cross section [22]. In addition, BNNTs retain high fracture toughness and flexibility [23], and tunable hydrophobic and wettability properties [24]. These properties make BNNTs a very attractive candidate for a reinforcement candidate in Al-MMCs.

The widespread study and use of BNNTs is limited when compared to that of CNTs. A review on the Scopus database for peer-reviewed publications shows the distinct delta

between the attention and research BNNTs receive when compared to that of CNTs (see Figure 4) [25]. One of the possible reasons for this is due to the hurdles in the large-scale production of BNNTs which require extremely high pressures and temperatures [26]. Other hurdles that production of BNNTs faces are the high host and relatively high toxicity that closely follows synthesis requirements [27]. However, due to the ever advancing field of material science, and the desire to fully understand the potential BNNTs could have, the production quality and quantity of BNNTs has seen a steady rise, and the now kilograms of BNNTs are readily available to the market [27].

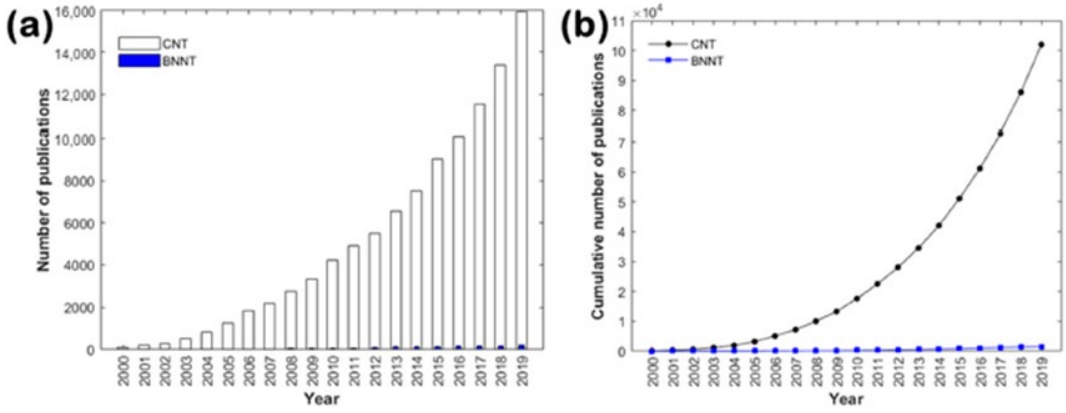

Figure 4. Scopus Search Results regarding BNNTs: (A) 2000-2019 Annual Peer Reviewed Publications CNT and BNNT (BNNT columns are hardly visible). (B) Cumulative number of CNT and BNNT publications (BNNT is blue line following horizontal axis). Source: [25].

BNNTs have a very similar crystalline structure to that of CNTs. Both BNNTs and CNTs have sp^3 bonded atoms form hexagonal rings for a tube-like structure [26], a seen in Figure 5. One of the most crucial differences between CNTs and BNNTs is the difference in electronegativity. BNNTs are comprised of polar covalent boron (B)–nitrogen (N) bonds, as opposed to CNTs who have covalent carbon (C) bonds only [25].

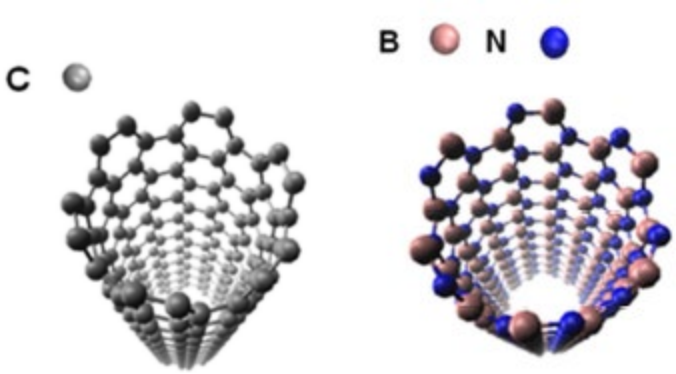

Figure 5. Structure of CNT (left) and BNNT (right). Source: [26].

Nanomaterials are materials that have a physical characteristic that has at least one dimension that is less than 100 nanometers (nm). With regards to BNNTs, the physical characteristic if the diameter of the tube, which when first characterized in 1995, was found to be between 1 and 3 nm with a total length of around 200nm [28]. Modern advances, especially when relating to production of BNNTs, have increased the length to nearly 200 micrometers (μm) [22]. As progress in production, study, and usage for BNNTs continues to advance, the limits for their application will continue to expand and evolve.

F. ALUMINA

Alumina is a ceramic and is one of the most common aluminum oxides. As previously discussed, ceramics are often added to MMCs to better the mechanical properties in the areas of hardness and wear resistance, features that ceramics are known for, while maintaining the properties of ductility and toughness, which is found in the metal. Because of these advantages, Al-MMC materials with alumina reinforcements are often preferred over unreinforced alloy materials [4].

There are other factors that make the use of ceramic-metal composite (cermets) materials advantageous besides the added mechanical properties the cermets provide. Specifically when dealing with cold spray, the addition of ceramic particles into the feedstock powder help to avoid nozzle clogging, therefore allowing the stagnation temperature to increase in the spray nozzle which in turn increases the deposition efficiency

of the coating [29]. Fernandez et al. also examined two additional mechanisms that the inclusion of ceramic particles aided to the overall deposition efficiency of the coating [29]. These mechanisms included the cleaning effect caused by oxide and the surface asperities creation caused when the ceramic particles impact the surface of the substrate. In another study by Irissou et al. that alumina when added at 20-30 volume percent to the aluminum powder, deposition efficiency increased by almost 300%. This same volume percent also showed that the porosity of the cold sprayed coating was reduced 1-7% [21]. The addition of alumina as a reinforcing particle has also been shown to be extremely beneficial to bond strength. Irissou et al. compared the bond strength of a pure aluminum coating to the bond strength of an aluminum coating with 10 vol. % alumina. The pure aluminum coating had values equal to 40 MPa bond strength and the aluminum coating with 10 vol. % alumina had a bond strength of 53 MPa. The vol. % was increased to 30% the bond strength increased above 60MPa, which was the rated adhesion pull for the epoxy used in the experiment [21].

Alumina has also been shown to significantly increase the hardness of cold sprayed coatings. Like the results for bond strength, an increase in the alumina content has shown to also increase the hardness of the coating. At coatings with higher alumina composition more ceramic particles will impact the coating but do not adhere to coating, which creates a peening affect to the already adhered coating, further increasing the work hardening [29]. Figure 6 shows the effect of increased alumina content has on coating hardness. Fernandez et al. found three zones as they related hardness to the wear resistance of coating with alumina content [30]. Specifically, that coatings containing 22 wt.% or less of alumina showed no significant benefit when compared to a pure aluminum coating. At higher values, a consistent increase in wear resistance is seen until 39 wt.% was reached.

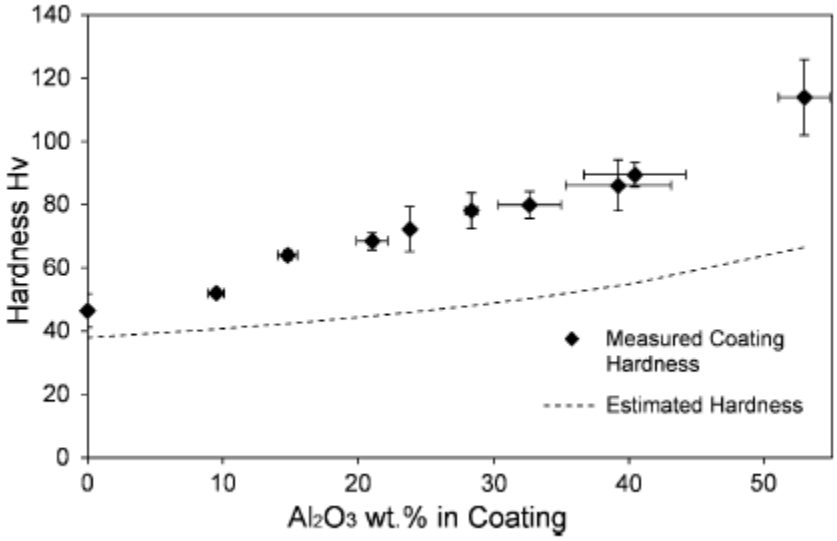

Figure 6. Measured and estimated hardness of coatings vs. coating alumina contents. Source: [30].

G. POWDER PROCESSING

When it comes to processing powders for the application of cold spraying, many methods have proven successful. Some of these methods include high energy ball milling (HEBM), solution ball milling (SBM), rotational milling modeling, shift-speed ball milling, and cryogenic mechanical milling [3]. The purpose of milling powders is to homogeneously mix the powders by placing the powders into a sealed metal container with proportionally weighted stainless-steel balls. The metal containers are then rotated or shaken at high revolutions per minute (RPM) for specific intervals to ensure that the powders are evenly distributed.

The development of HEBM was to combine the beneficial properties of "high-temperature oxide dispersion hardening with low-temperature precipitation hardening in nickel alloys" [31], which soon after led to the production of metallic powders and intermetallic alloys [32]. HEBM has also shown to reduce the size of ceramic particles to the nano regime for the use in various chemical processing techniques as well as having the ability to reinforce aluminum powders with nanodiamond powders, which ultimately increased the hardness and wear resistance properties of the composite powder [33], [34].

There are several parameter factors that affect the powder particle properties when HEBM is employed, two of these parameters are ball-to-powder ratio (BPR) and milling times. Woo et al. investigated the BPR on properties such as hardness and discovered that when BPR was increased the hardness values of the milled powders increased as long as the milling times were kept under 2 hours [35]. Rice found that a BPR of 1:5 when milling pure aluminum with graphene nanoplatelets and boron carbide in 5 minute intervals for a total milling duration of 100 minutes produced powder morphology that was most ideal for his cold spray application onto aluminum substrate [13].

Ansell et al. explored different parameter spaces for which HEBM could be used to process particulates without a significant loss of shape to powder particles. It was determined that powder morphology is more apt to be affected with changes in BPR, specifically a higher BPR yielded flattening of metallic particulates [31]. Figure 7 visually shows that an increase in BPR coupled with an increase in the number of cycles increases the flattening of the particles. HEBM, when implemented properly, specifically the parameters of BPR and interval milling times, is an ideal choice for producing MMC powders that can effectively be implemented into cold spray applications.

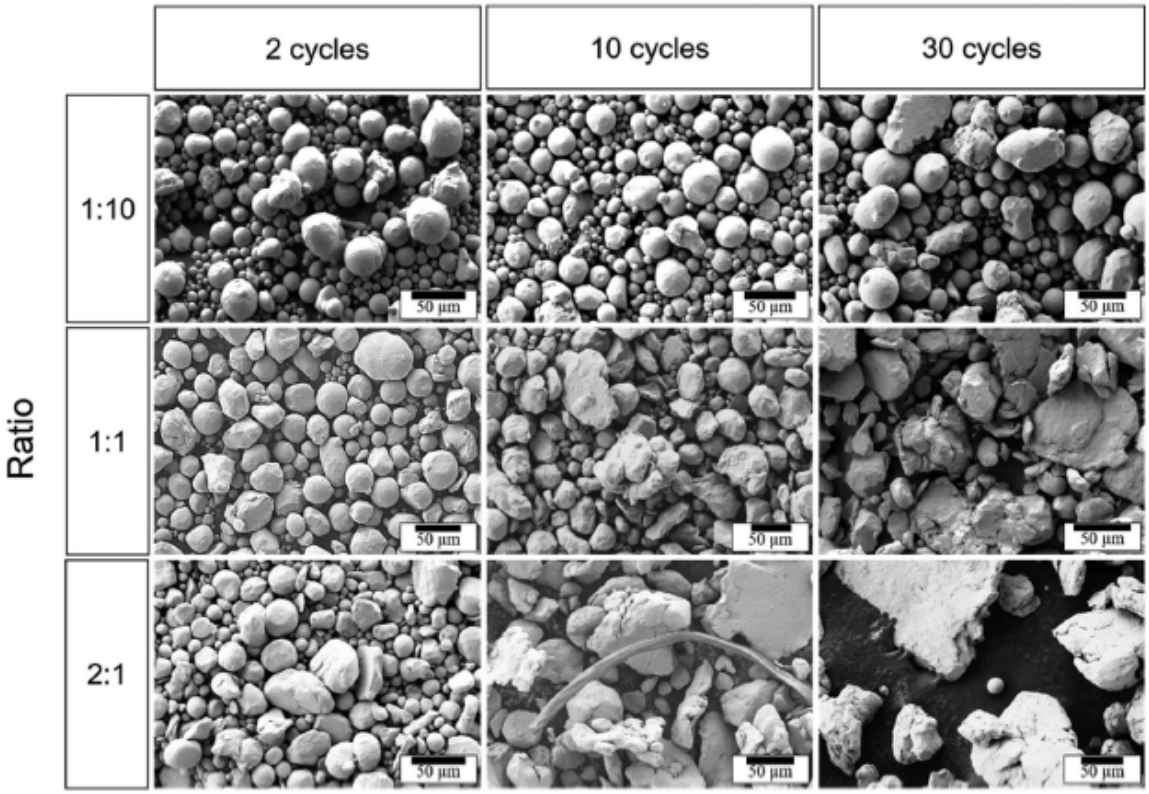

Figure 7. HEBM effects on 316L stainless steel powders. Source [31].

III. EXPERIMENTAL METHODS AND PROCEDURES

A. MATERIALS SELECTION

The base metal matrix that was used throughout the course of this study was Al-7075. Al-7075 was chosen as the base metal because of its material properties, specifically its good resistance to corrosion. Additionally, Al-7075 is commonly used in the aerospace industry due to its light weight and strength properties. With the ever increasing development of the aerospace industry, Al-7000 series alloys, especially Al-7075, are expected to display high marks in several material properties categories [36]. For these reasons, Al-7075 makes a good candidate to use as the base metal metric in cold spray applications as well as the use of ceramics as reinforcements in the matrix.

The Al-7075 powder used in this experiment was sourced from Valimet, Inc., located in Stockton, California (Batch No. 19-002s). The Al-7075 particles, as received from the manufacturer, were stated to be spherical and 15-53 μm in size. Particles as received from the manufacturer are seen in Figures 8 and 9. The shape of the average particle was spherical, and the size of the particles were in the range as prescribed by Valimet, Inc. It is possible that the shape and overall morphology of the powder could be affected by the HEBM process, but the goal here is for the morphology of the spherical Al-7075 is to remain unchanged.

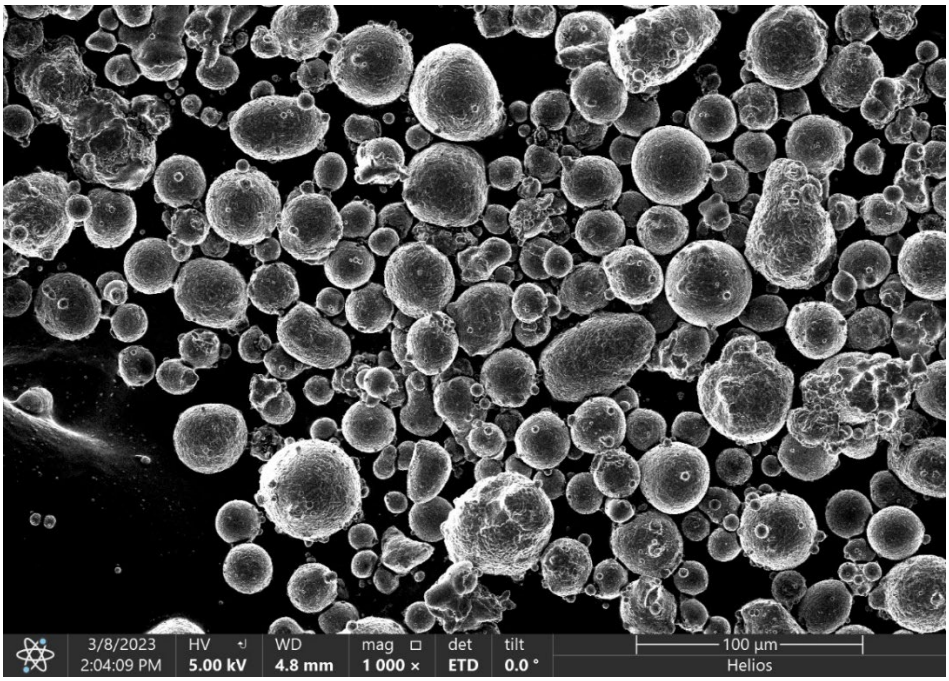

Figure 8. Al-7075 powder as received from manufacturer 1kX magnification

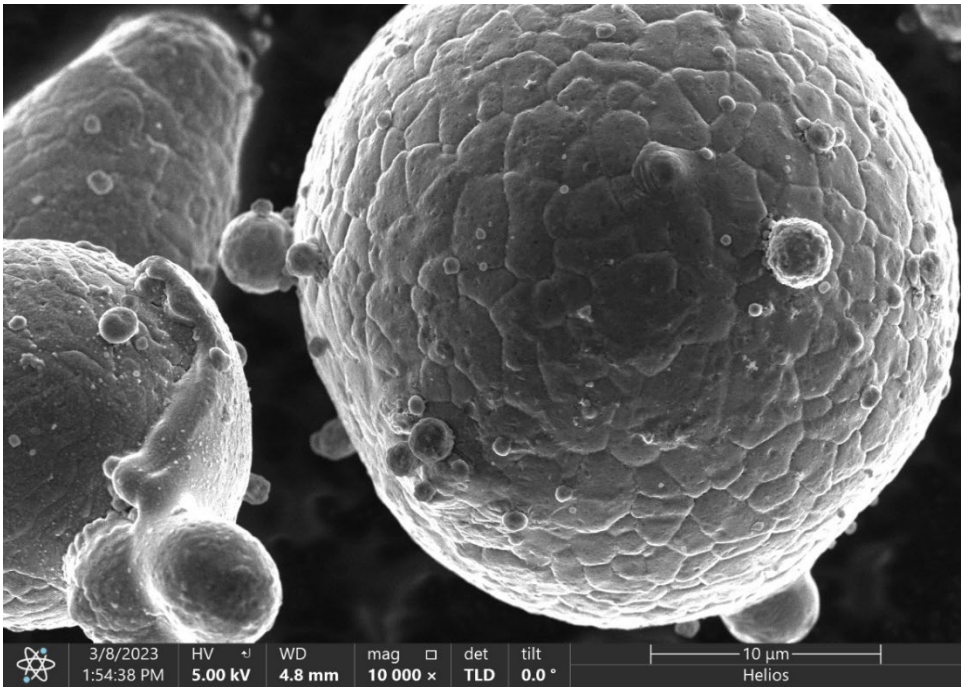

Figure 9. Al-7075 Powder as received from the manufacturer 10kX magnification

B. METAL MATRIX COMPOSITE

The two ceramic particles that were chosen to reinforce the Al-7075 metal matrix were alumina and BNNTs, as previously discussed in Chapter I. The alumina was sourced from Alfa Aesar (Lot No. B21X017). The purity of the alumina, as stated from the manufacturer, is 99.97% and ranges from 1 to 3 μm in particle size and has a specific area of 80-120 m^2/g [37]. The alumina particles appear to be orientated in irregular fiber bundles, as seen in Figure 10, and when viewed under an SEM electron charging of the particle is likely to occur, which can make distinguishing the alumina from the Al-7075 easier, as seen in Figure 11.

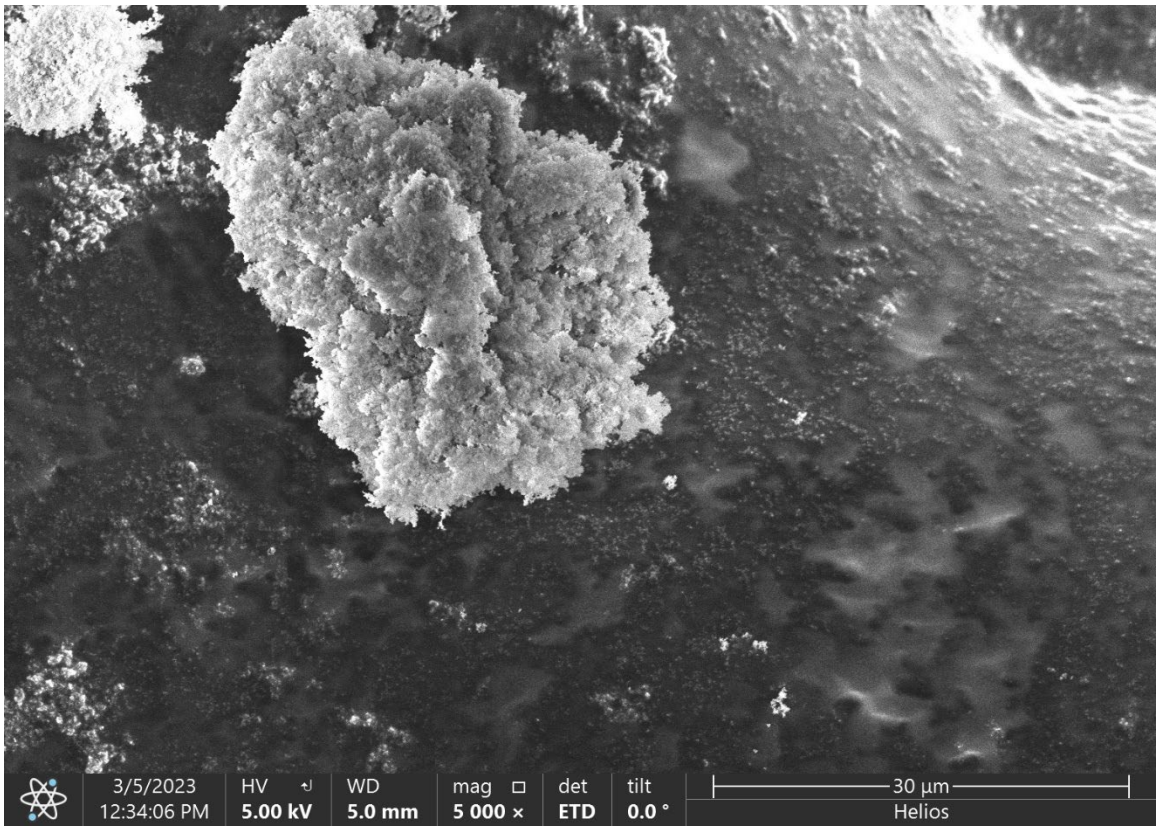

Figure 10. Alumina as received from manufacturer

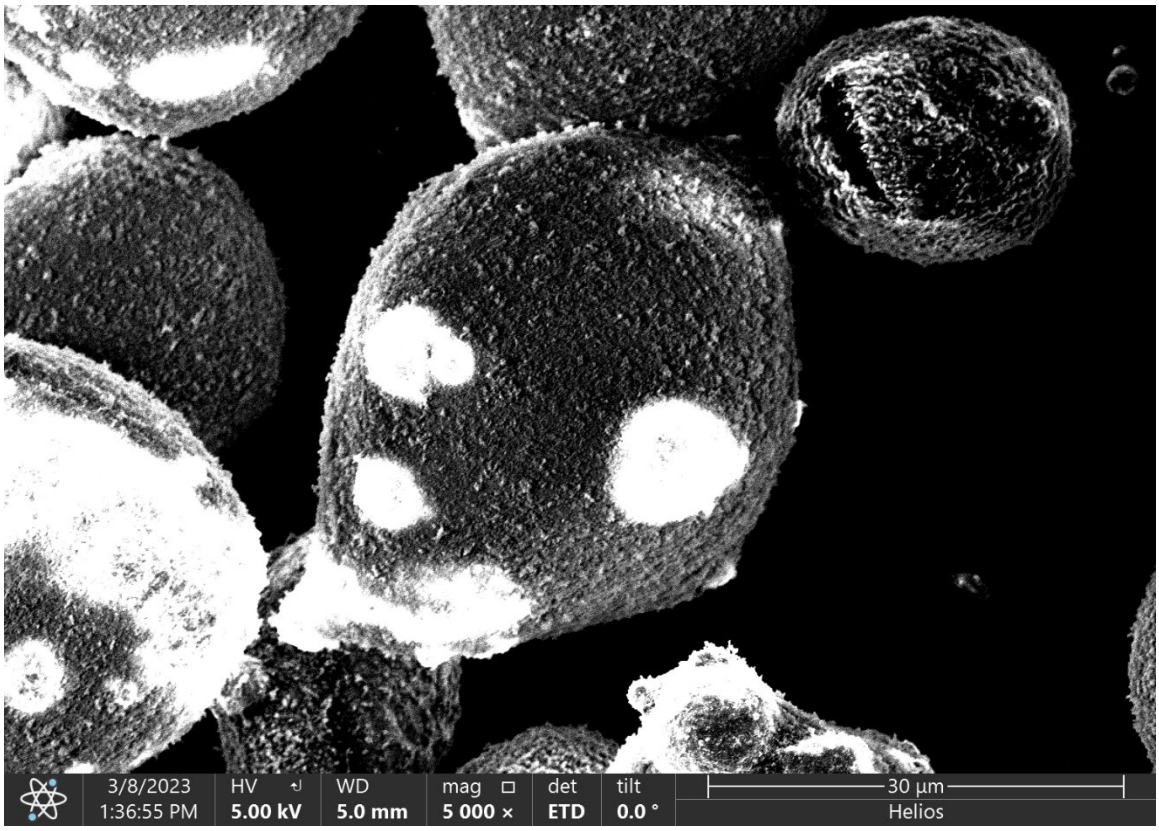

Figure 11. Alumina particles adhering to Al-7075 post HEBM

The BNNT ceramic reinforcements that was used in this study were sourced from BNNano (BNNP-P-90A1). Literature often describes BNNTs as "boron nitride nanobarbs" [38]. The manufacturer refers to BNNTs as nanobarbs because of the barb-like structures that appear on the wall of the BNNT when viewed at the nano scale, as seen in Figures 12 and 13. It should be noted that boron nitride nanotubes and boron nitride nanobarbs are synonymous, however, boron nitride nanotubes (or BNNTs) will be used throughout the course of this study.

Figure 12. TEM image of a BNNT, as received from the manufacturer. Source: [3].

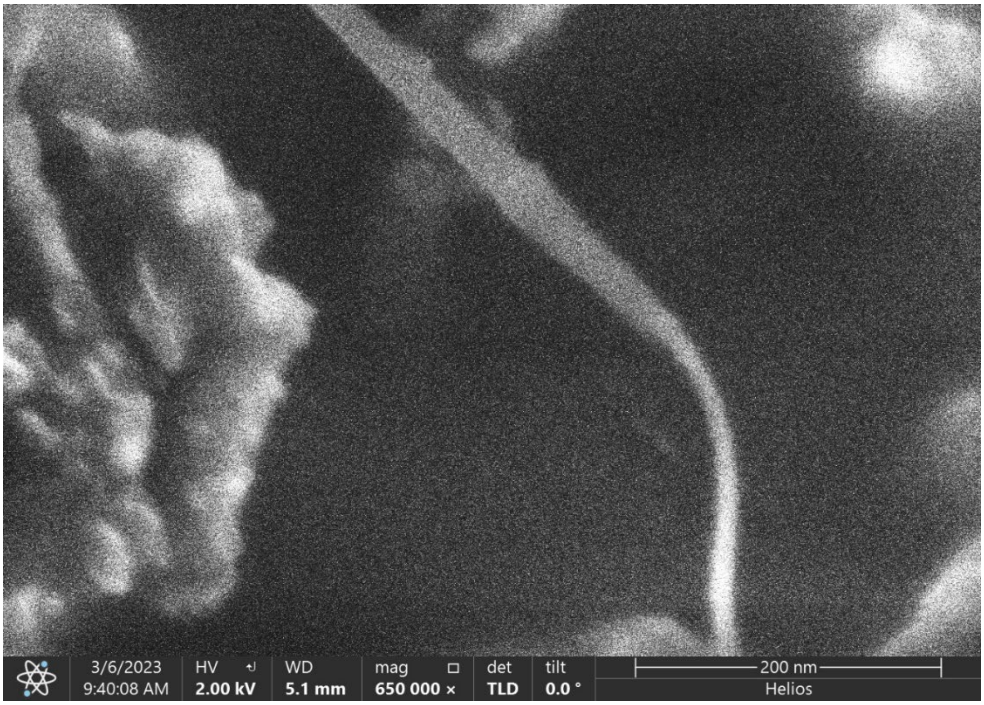

Figure 13. SEM image of BNNT agglomerations, as received from manufacturer

C. ALUMINUM 7075 SUBSTRATE

The substrate material to was employed for this study was Al-7075 alloy. The substrate originated in plate form, from there it was machined into 25mm wide, 152mm long, and 6mm deep bars to facilitate the application of cold spray coating and further mechanical testing of coatings. The Al-7075 alloy is comprised of the elements shown in Table 1.

Table 1. Al-7075 alloy. Elemental composition in wt%. Source: [39].

Zn	Mg	Cu	Cr	Si	Mn	Fe	Ti	Al
5.78	2.46	1.75	0.262	0.187	0.143	0.126	0.175	Balance

Al-7075 alloy is a part of the Al-Zn-Mg-Cu series of Al- alloys. It was chosen for this study because of its high strength, toughness, and thermal deformation performance, and is one of the principle materials employed in the aeronautics industry [39]. A cold sprayed coating, utilizing Al-7075 for its already discussed material properties, BNNTs for their temperature stability and electrical insulation properties, and alumina for its hardness and wear resistance properties, could potentially increase the service life of many materials used in the aerospace industry.

D. HIGH ENERGY BALL MILLING

The purpose of grading layers of MMCs is to extract the properties you desire for your coating and apply them at the correct interface of the coating layers. For this reason, several compositions containing alumina, Al-7075, and BNNTs were milled together using varying vol.%, as seen in Table 2.

Table 2. Cold spray coating compositions

Material ID	Al-7075 vol.%	Alumina vol.%	BNNT vol.%
Al-7075	100	0	0
Al-7075/Alumina	90/80/70	10/20/30	0/0/0
Al-7075/BNNT	98	0	2
Al-7075/Alumina/BNNT	89	10	1

Each of the compositions were calculated using the densities provided by the respective manufacturer. These densities are recorded in Table 3.

Table 3. Powder densities

Powder	Density [g/cm^3]
Al-7075	2.81
Alumina	3.95
BNNT	2.29

HEBM was employed to fabricate all powders sprayed in this study. The process of HEBM, as discussed in Chapter II, involves the use of high strength metal canisters in which the weighed and proportioned powders are mixed with a 1:5 weight ratio of stainless-steel milling balls and shaken at high RPMs for prescribed time intervals. This process allows the mixed powders to deagglomerate and cold weld together. The final Al-7075 powder, after the HEBM process, should retain the original spherical shape as prior

to milling process as well as have the ceramic reinforcements even distributed out respective to the volume fraction that introduced.

The HEBM process was conducted using the SPEX SamplePrep Mixer/Mill 8000D and operated at 1060 cycles per minute. A previous study by Rice found that a BPR of 1:5, with cycling the on/off intervals every 5 minutes for a total of 10 intervals produces powders that were uniform in distribution and retained their original morphology [13]. Using these parameters, composite powders that exhibited ideal characteristics for the cold spraying process were produced.

Ideally, when conducting HEBM, maximizing the amount of powder during the milling process is preferred. However, due to the varying volume percentages of the alumina, and physical characteristics of the as received alumina powder from the manufacturer, it was not feasible to mill large quantities at one time. Instead, when milling alumina with Al-7075, the total weight of the mixture had to be reduced while reflecting the correct vol.% of the mixture. Specifically, 30 g, 40 g, and 50 g alumina in the 10 vol.%, 20 vol.%, and 30 vol.% powders, respectively, could be mixed with Al-7075 in one canister at a time. Each mixture would still maintain the same BPR of 1:5. Typical parameters are given for a HEBM cycle when milling 10 vol.% alumina with Al-7075 in Table 4.

Table 4. HEBM parameters for Al-7075 w/ 10 vol.% alumina

Powder Mass	Milling Media	Containment Vessel	BPR	Interval Time	Total Cycles
50g	3 mm 504 SS Balls	SS Canister	1:05	5 min on/5 min off	10

E. COLD SPRAYING

All five compositions that were milled using HEBM were then transferred to glassware and placed into an oven at 75°C for a minimum of 12 hours to remove any residual moisture that might remain in the sample.

The Al-7075 substrate was prepared prior to spraying to best allow for particle adhesion during to the cold spray process. Literature discussing cold spray substrate preparation has variation on what process best allows for particle adhesion. Two common practices are grit blasting and sanding the substrate. Singh et al. [40] noticed little difference in deposition efficiency and particle adherence to the substrate when comparing these two methods. The substrate preparation process in this study consisted of sanding the substrate bars with 320 grit sandpaper to remove the oxidation layer, then subsequently sanding with 600 and 800 grit sandpaper to ensure that that the oxidation layer had been removed. Once the sanding was complete, the bars were wiped down with ethanol to remove any excess debris that might be present and then dried under a heat gun to remove any moisture.

The equipment that was used to cold spray the Al-7075 substrate was a Centerline Supersonic Spray Technologies (SST) Series P Spray Machine, with an X-Feeder, and a Series P Automatic Spray Gun. As discussed in Chapter II, nitrogen was chosen as the carrier gas. The cold spray process relies on the use of a converging-diverging de Laval supersonic nozzle. The nozzle used in this study was made of a polymer, which ultimately clogged less frequently than metal alloy nozzles, providing more consistency during the powder feed process.

Before spraying coatings that would undergo mechanical testing, the cold spray parameters were parameterized to best optimize not only the deposition efficiency of the coating but the coatings porosity and uniformity. Previous studies conducted similar tests and their cold spraying parameters were used a baseline until final optimized parameters were established [3], [13]. Because this study was exploring the effects of graded coating layers, which required multiple coats with different ceramic particles at varying volume percentages, it was determined that the optimized parameters should be a best fit model for each individual spraying process. These best fit parameters would not only facilitate the ease of spraying, but also reduce the cool down time of the as sprayed coating before the next coating layer was deposited, ultimately increasing deposition efficiency and particle adhesion [10]. The final spraying parameters are recorded in Table 5.

Table 5. Final spraying parameters

Nozzle Temperature	Gas Pressure	Standoff Distance	Feed Rate	Traverse Speed	Line Spacing
425°C	1.7 MPa	12.7 mm	9.7 g/min	20 mm/s	1 mm

Figure 14 shows the visual results of the cold spray trials. Upon visual inspection, the coatings all appear to be very uniform and does not have noticeable porosity or surface defects. The coatings do appear homogeneous. The coatings were cross-sectioned and an optical microscope was used to determine approximate porosity and coating thicknesses.

Figure 14. Top-down view of cold spray coatings

F. SAMPLE PREPARATION AND STORAGE

Once all coatings had been sprayed, samples were cross-sectioned using a Struers Secotom-20 high speed saw, as seen in Figure 15. Once cross-sectioned, the samples were then mounted into conductive epoxy pucks using a Struers CitoPress-10, as seen in Figure 16. All heating and cure times for the sample puck mounting were done in accordance with manufacturer's specifications. Once the cross-sectioned samples were successfully mounted they were polished and characterized under the SEM. The polishing process was conducted using previously established parameters used by Tauber [3]. Table 6 details the parameters that were used in each step of the polishing process. The end goal was to have a near mirror finish on the cross-sectioned sample to facilitate the proper microscopy characterization. After the final polishing was complete, each sample was chemically etched to provide surface and microstructural contrast. The chemical etching agent that was utilized was Keller's reagent which adequately corroded the particle splat boundaries [41]. Figure 17 shows an unpolished sample cross-section mounted in conductive epoxy resin and Figure 18 shows a polished puck mounted in the same conductive resin.

Table 6. Polishing parameters

Step No.	Grit/Solution	Time	RPM
1	320	5 min	250
2	500	10 min	250
3	800	15 min	250
4	1200	15 min	250
5	1 µm Alumina	30 min	250

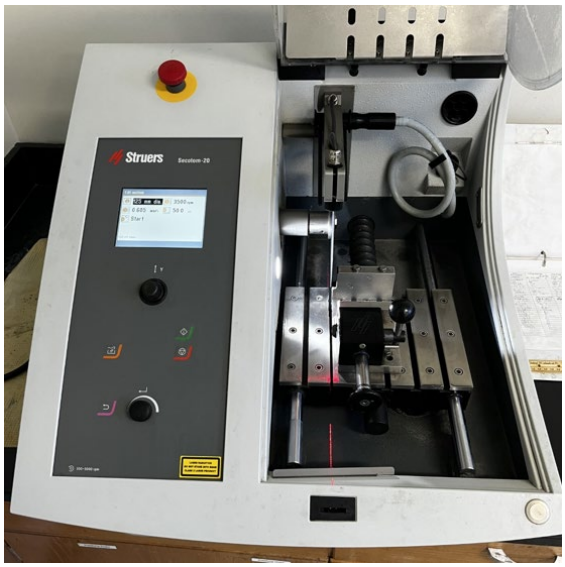

Figure 15. Struers Secotom-20

Figure 16. Struers CitoPress-10

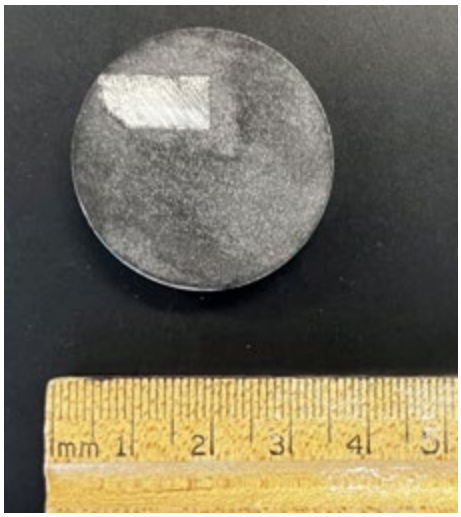

Figure 17. Unpolished puck

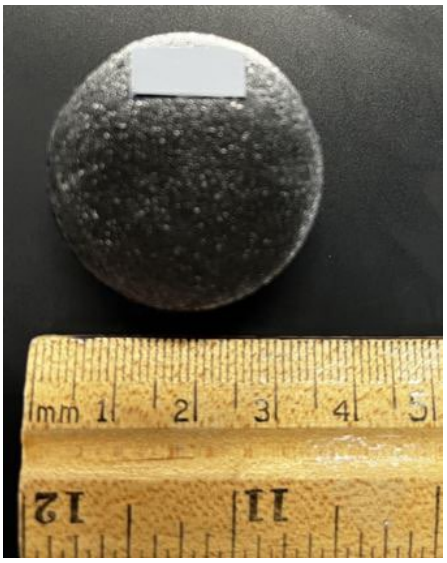

Figure 18. Polished puck

Aluminum exposed to ambient conditions is susceptible to oxidation and because of this all samples were stored when not being utilized for mechanical testing or microscopy. The storage that was used to minimize the possible effects of oxidation were a SECADOR Desiccator or a PELCO 2251 Vacuum Desiccator.

G. MECHANICAL TESTING

1. Adhesion

The adhesion strength was tested for each of the four compositions. There were also four adhesion control tests conducted that did not include graded coatings. The three control adhesion tests were conducted with a coating composition of Al-7075 with 10, 20, and 30 vol.% of alumina respectively, as well as Al-7075 with 2 vol.% BNNTs that was applied directly to the substrate. Table 7 details the adhesion test coating compositions and their respective graded layers compositions. All adhesion tests were conducted in accordance with (IAW) American Society for Testing and Materials (ASTM) D4541 standard. The number of adhesion tests varied from three to five tests, which were dependent on material availability and failed tests due to glue up failure. Each test was conducted using an Elcometer 510 Model T automatic tension tester, 10 mm dollies, and Master Bond EP15ND-2 epoxy. Elcometer 510 Model T was programmed to pull at a constant rate of 1.03 MPa (150 psi) per second, with the final stress value upon adhesion failure being displayed digitally. The Master Bond EP15ND-2 epoxy is a single component epoxy. The epoxy requires heat curing and has a tensile strength that is near 82.7 MPa. The curing requirements for the epoxy were 150-177°C for 90 minutes [42]. The epoxy was cured in a Quincy Lab, Inc Model 10 Lab Oven. Table 8 details the adhesion testing parameters that were used.

Table 7. Adhesion coating sample compositions

Sample Number	Base Layer Composition	Mid-Layer Composition	Top Layer Composition
1 (CONTROL)	98 vol. % Al-7075 / 2 vol. % BNNT	N/A	N/A
2 (CONTROL)	10 vol.% Alumina / 90 vol.% Al-7075	N/A	N/A
3 (CONTROL)	20 vol.% Alumina / 80 vol.% Al-7075	N/A	N/A
4 (CONTROL)	30 vol.% Alumina / 70 vol.% Al-7075	N/A	N/A
5	98 vol. % Al-7075 / 2 vol. % BNNT	N/A	10 vol.% Alumina / 90 vol.% Al-7075
6	98 vol. % Al-7075 / 2 vol. % BNNT	N/A	20 vol.% Alumina / 80 vol.% Al-7075
7	98 vol. % Al-7075 / 2 vol. % BNNT	N/A	30 vol.% Alumina / 70 vol.% Al-7075
8	98 vol. % Al-7075 / 2 vol. % BNNT	89 vol. % Al-7075 / 10 vol.% Alumina / 1 vol. % BNNT	30 vol.% Alumina / 70 vol.% Al-7075

Table 8. Adhesion test parameters

Pull Rate (MPa/sec)	Dolly Size (mm)	Cure Temp (°C)	Cure Time (min)	Ambient Temp (°C)
1.03	10	171	90	23

After the conclusion of all adhesion tests, all stress failure data was gathered, and adhesion failure surfaces were analyzed and classified by their failure modes. The possible failure modes include delamination or adhesion failure (failure at the substrate), cohesive

failure (within the coating itself), or glue failure (failure of clue to bond to dolly and coating).

2. Wear Testing

Wear testing was conducted to determine the resistance of the coating to deterioration over time. With the application of graded coatings, the only coating to be immediately susceptible to wear would be the topcoat, therefore the wear tests that were conducted for this study only applied to samples that had different compositions on the top layer of the cold spray coating, to include the final functionally graded cold spray.

Wear resistance tests were conducted in a series of three ball-on-disk dry sliding wear tests. All samples that were tested had a topcoat that consisted of two layers of cold spray coating, this was to ensure that the depth of coat was sufficient to last the duration of the wear test. All wear tests were conducted on the surface of the coating and not on the samples cross-section. The parameters for the wear tests are detailed in Table 9. The mechanism for conducting the wear tests was a Nanovea T50, a modular tribometer, as seen in Figure 19. Prior to conducting the wear tests, each sample was sectioned off from a larger sample using a Struers Secotom-20 high-speed saw (as seen previously in Figure 14) to facilitate placement in the tribometer. The mass of the sectioned samples was measured before and after each test to determine mass loss. The surface that induced the wear for this test was a 3 mm stainless steel 304 ball. During testing, the depth of the wear was measured via the tribometers encoder, which also recorded the coefficient of friction in real-time. The data collection rate for both the coefficient of friction and depth was set to 20 data points per second. The applied load for the tests was 1N, and the wear tracks were 3 mm in diameter. The sample was rotated at 100 RPM for 1 hour, which resulted in a total sliding distance of 56.5 m.

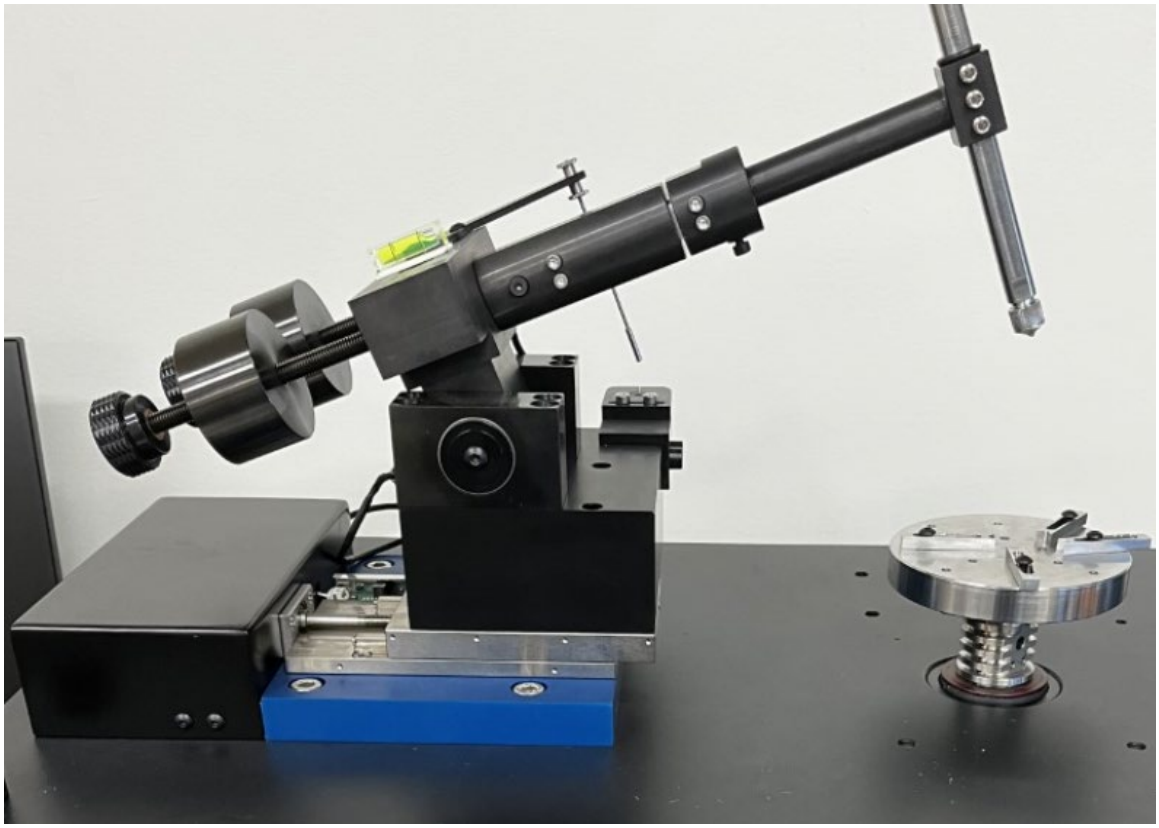

Figure 19. Nanovea T50 tribometer

Table 9. Wear testing parameters

Test	Applied Load (N)	RPM	Test Duration (min)	Wear Track Diameter (mm)	Total Sliding Distance (m)	Counter Surface
Ball-on-Disk	1	100	60	3	56.5	3 mm SS 304 Ball

H. CHARACTERIZATION

All powders and all sprayed samples underwent microscopic inspection. All powder samples were mounted onto SEM sample stubs using specialized double-sided carbon tape and placed in proper storage (as detailed previously in this Chapter) until SEM analysis could be conducted. All cross-sectioned samples were suspended in an epoxy puck

using Struers ConduFast epoxy powder. ConduFast is an electrically conductive resin which contains iron powder filler for optimal conduction when using electron microscopes. ConduFast epoxy was used because alumina and BNNTs can cause samples to charge when being analyzed under an SEM. ConduFast, with its iron filler powder, allows a more unobstructed path for the electrons when the beam column is operating at higher beam voltages during SEM operations.

Prior to being analyzed in the SEM, all mounted samples were examined using a Nikon Model Epiphot 200 Microscope equipped with a Nikon Digital Sight DS-2Mv. The lower magnification, which ranges from 2.5 to 100 times in light and dark fields, of the Nikon microscope was used for visual inspections of samples before being placed into an SEM for further analysis.

The two electron microscopes that were utilized in this study were the Zeiss Neon 40 SEM and the FEI Helios 5 UX SEM, as seen in Figure 20 and 21. The two SEMs are capable of examining samples at very high magnifications. Parameters for analysis during SEM operations varied depending on the composition of the sample and the purpose of the analysis. Electron beam voltages ranged from 2kV to 30kV with multiple different working distances. Some electron optical and detection features were utilized, such as immersion mode, backscatter electron detector, secondary electron detector, beam deceleration mode, through-lens detector (TLD), and Everhart-Thornley detector (ETD).

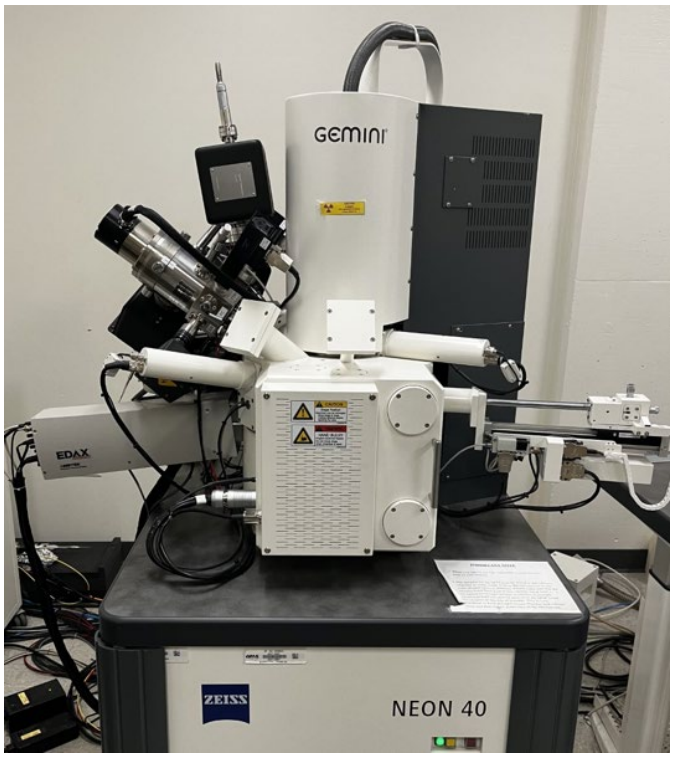

Figure 20. Zeiss Neon 40 SEM

Figure 21. Helios 5 UX SEM

THIS PAGE INTENTIONALLY LEFT BLANK

IV. RESULTS AND DISCUSSION

A. POWDER COMPOSITION AND CHARACTERIZATION

All powder compositions that were created using HEBM were analyzed under the SEM. Each powder was imaged to ensure the Al-7075 spherical morphology was relatively unchanged and that the ceramic reinforcements were adequately and evenly distributed throughout the composition.

1. Al-7075 and BNNT Powder

The Al-7075 as received from the manufacturer was imaged and then compared to the Al-7075 with BNNT post HEBM to compare the effects of the milling process on the Al-7075 morphology as well as ensuring the proper dispersion of BNNT particles. The Al-7075 received from the manufacturer can be seen in Figures 8 and 9. The Al-7075 with BNNTs post HEBM are seen in Figure 22. An agglomeration of BNNTs with Al-7075 particles adhered to the surface can be seen circled in red.

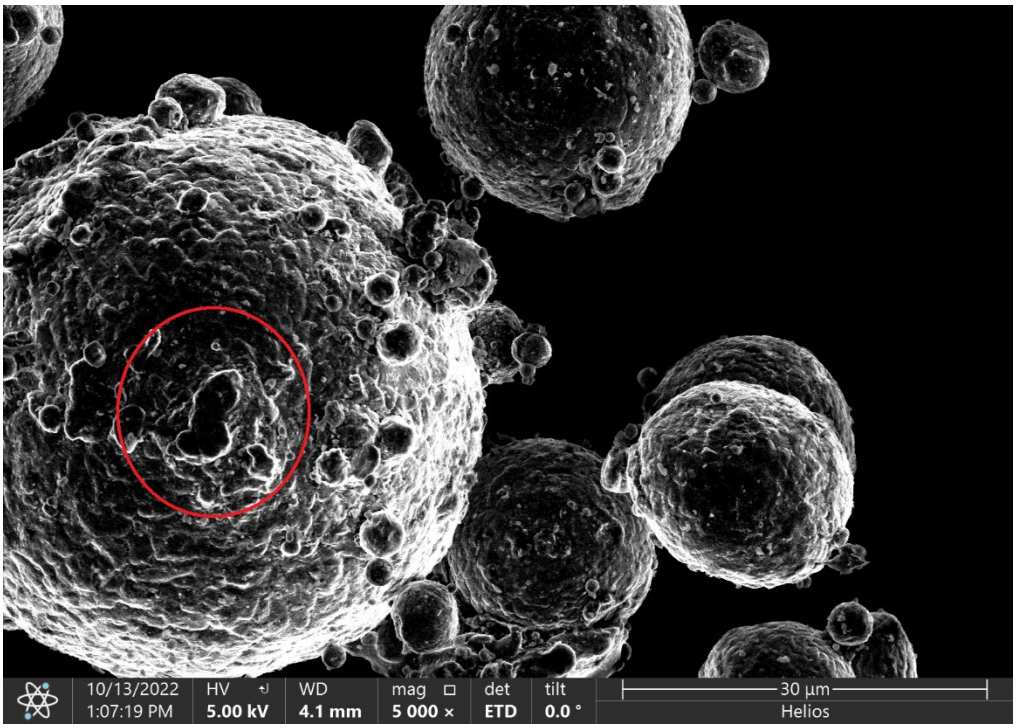

Figure 22. Al-7075 and BNNT post HEBM

Figure 23 shows that the Al-7075 particles remained spherical with little evidence of extensive plastic deformation post HEBM. The BNNTs did agglomerate after ball milling. Finding individual BNNT particles was difficult due their size and overall volume percentage within the composition. The easiest way to determine the presence of BNNTs during SEM imaging was to find an agglomeration and then locate individual particles on the surface of nearby Al-7075 particles. Figure 24 shows an agglomeration of BNNTs that was located, and Figure 24 shows an individual BNNT that was located on the surface of a nearby Al-7075 particle.

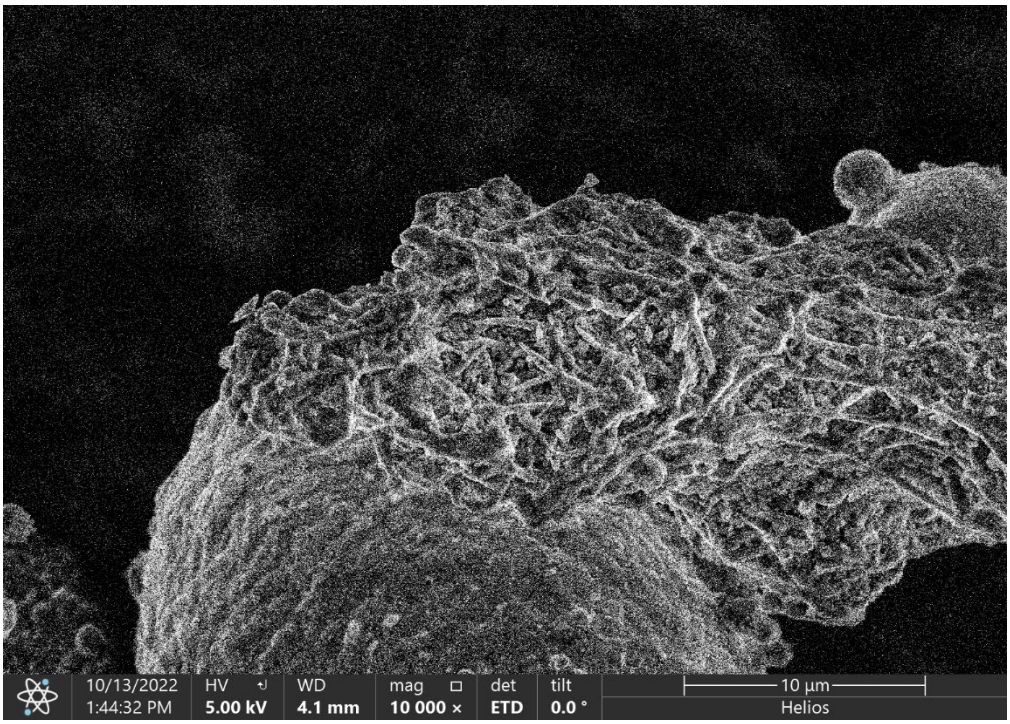

Figure 23. Agglomeration of BNNTs within Al-7075 post HEBM

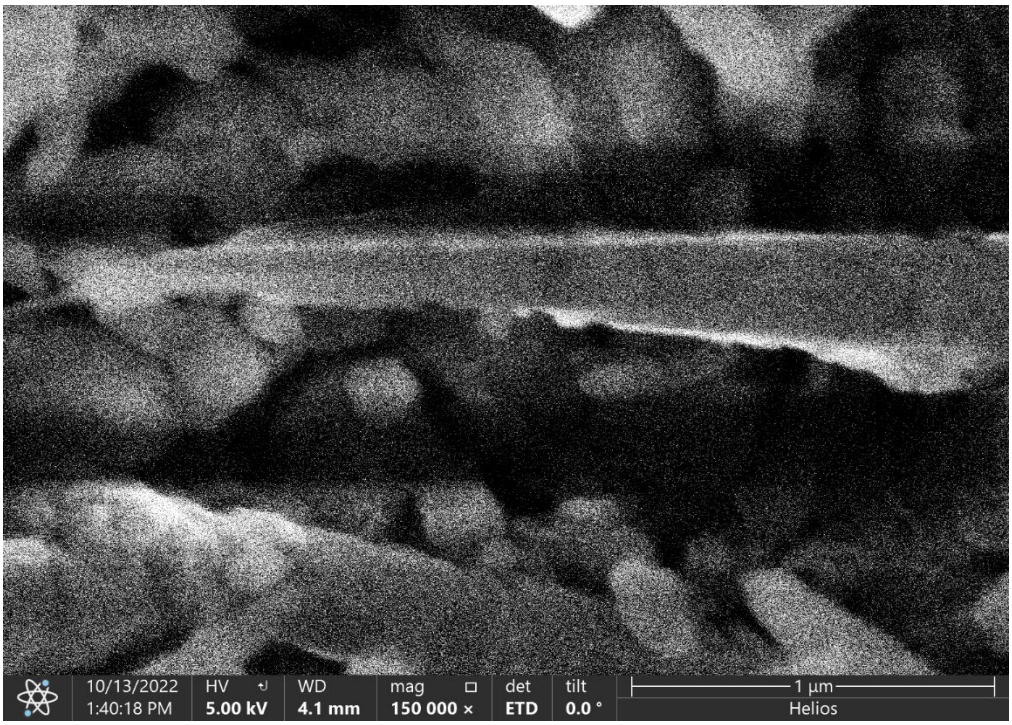

Figure 24. Individual BNNT located on surface of Al-7075 particle

2. Al-7075 and Alumina Powder

Three separate Al-7075 powders were mixed via HEBM with volume percentages of 10 vol.%, 20 vol.%, and 30 vol.%. Each of these compositions were examined under the SEM to determine proper morphology of the Al-7075 as well as adequate dispersion of the alumina through the composition. Figures 25, 26, and 27 show the Al-7075 and alumina at 10 vol.%, 20 vol.%, and 30 vol.% respectively. The alumina in all volume percentages was dispersed throughout the matrix and was located on the surface of the Al-7075 powder, with minimal agglomerations of solely ceramic particles. The majority of these agglomerations of alumina occur where the ceramic is causing a bond between individual Al-7075 particles. The alumina acts as an adhesive.

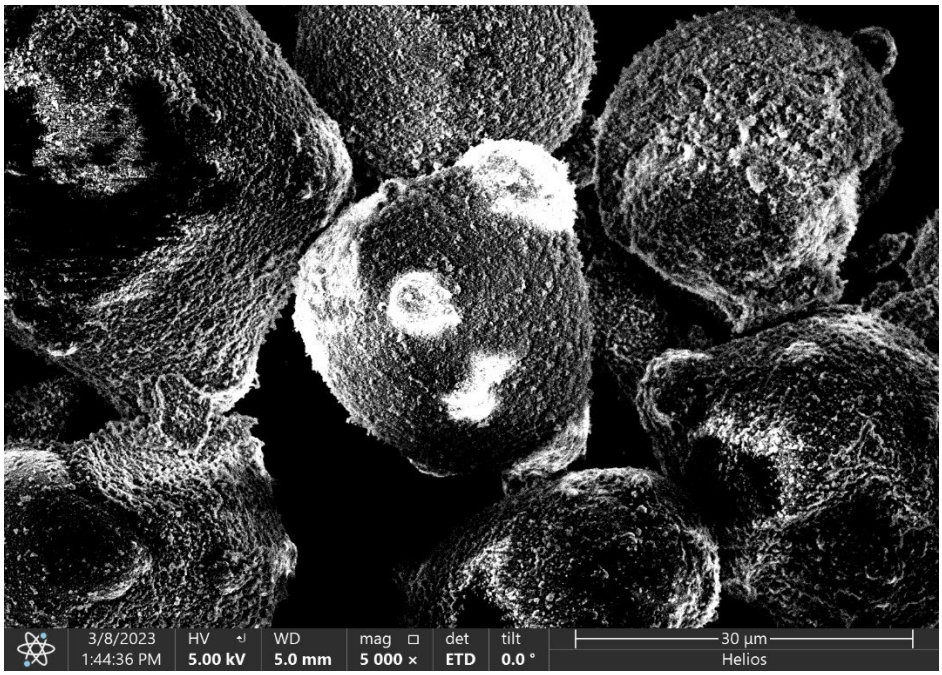

Figure 25. SEM Image of Al-7075 with 10 vol.% alumina

3. Al-7075, Alumina, and BNNT Powder

Figure 26 shows a lower magnification image of powder that contains Al-7075, BNNTs, and alumina as the reinforcing ceramics. As seen in Figures 23 and 26, the Al-7075 particles seem to retain much of their spherical morphology post HEBM.

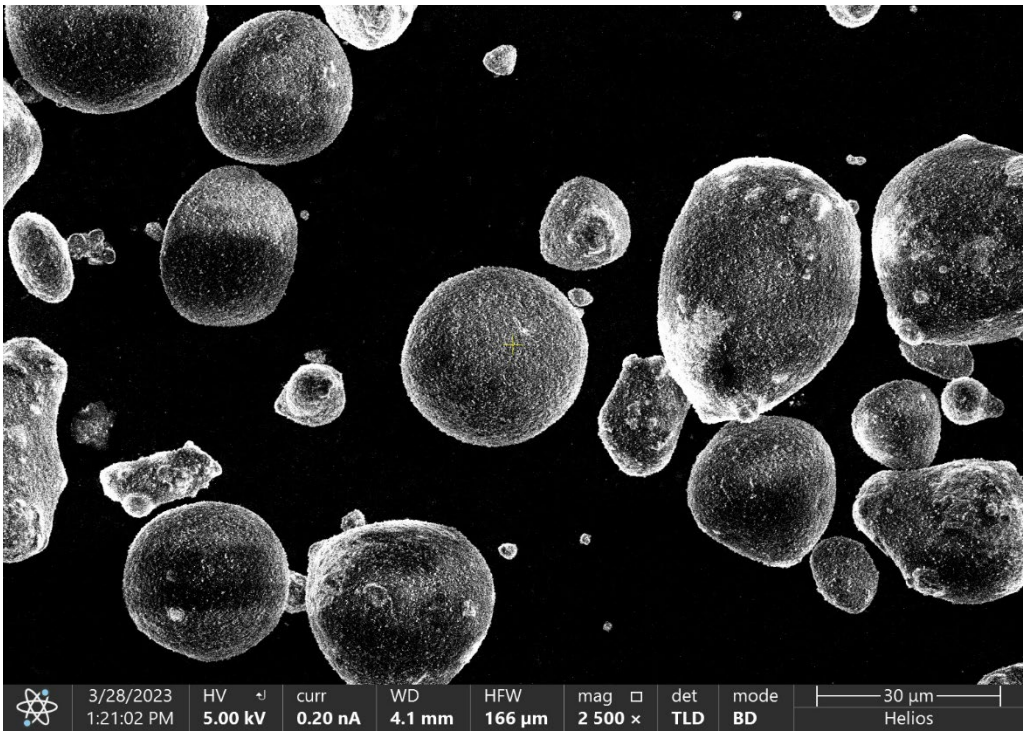

Figure 26. Al-7075, BNNT, and Alumina powder post HEBM

It can be seen in Figure 27 that many of the same results occurred between the alumina and Al-7075 particles where the alumina will bridge two Al-7075 particles together, acting as an adhesive. In Figure 26, the through lens detector was used in the SEM with a decelerated electron beam creating electron charging of the alumina particles, which made distinguishing the alumina particles easier for the powder characterization.

Figure 28 shows a 5 µm diameter Al-7075 particle connected to a larger Al-7075 particle via alumina. Figure 28 displays several Al-7075 particles that have alumina bridges between them. Selected alumina bridges have been circled in red.

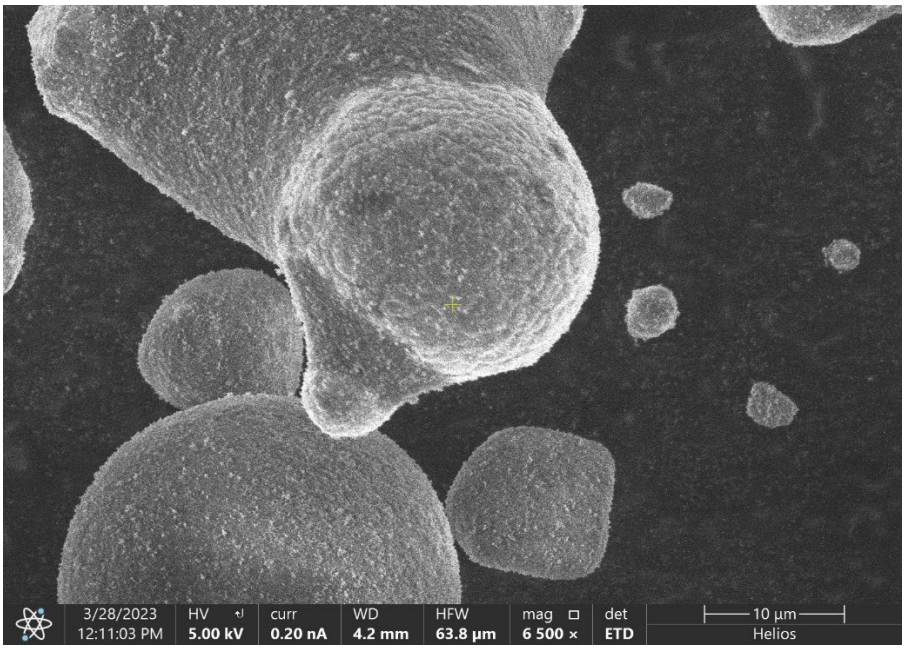

Figure 27. Two Al-7075 particles bridged with alumina

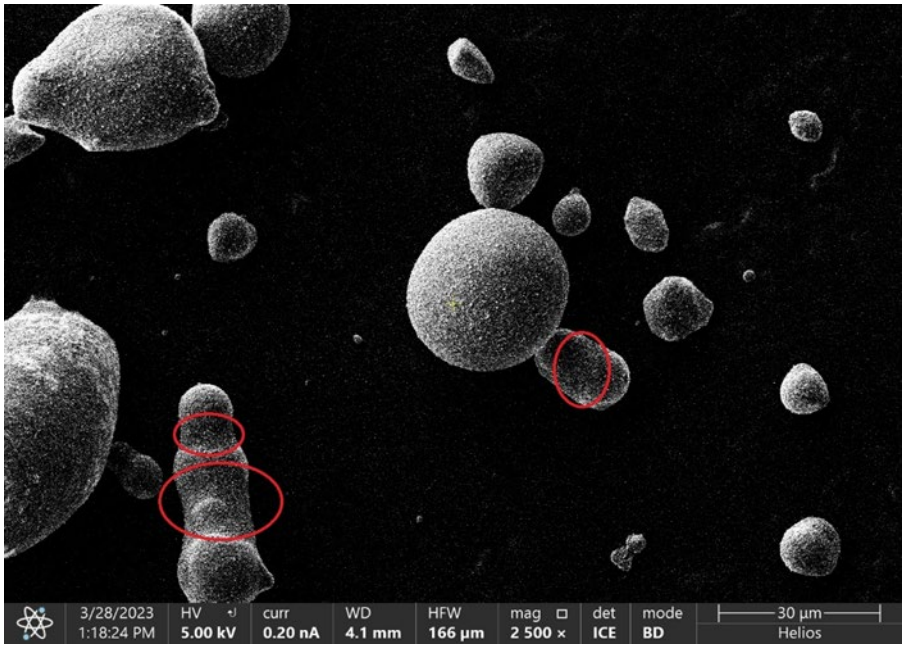

Figure 28. Alumina bridging several Al-7075 particles as seen circled in red

Figure 29 shows a magnified image of an Al-7075 particle, which has alumina adhered to the surface. Comparing the SEM imagery pre- and post-HEBM shows that the

alumina appears to have adequate dispersion within the MMC. As seen in Figure 29, the alumina appears to have been milled to smaller particle size allows for a more through distribution of the previous agglomerations that were present in the as received alumina powder.

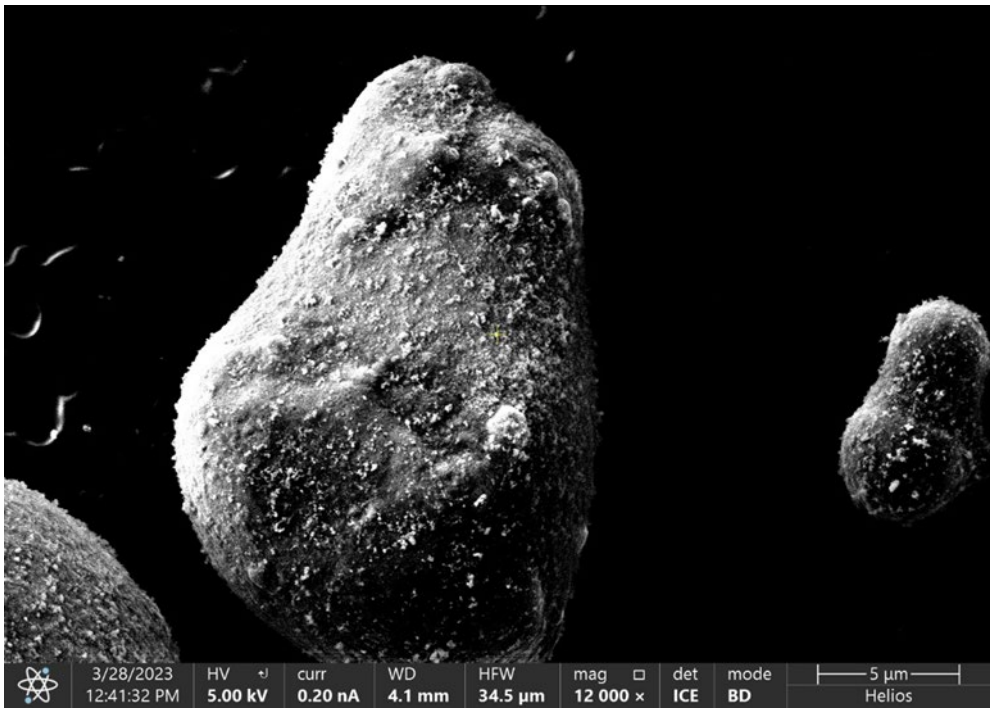

Figure 29. Surface adhesion of alumina on Al-7075 particle

The previous agglomerations of BNNTs that were present in powders pre HEBM seemed to be completely dispersed, no agglomerations were found during SEM of the powder containing Al-7075, BNNTs, and alumina. However, individual BNNTs were found to be present within the powder. Figure 30 shows the Al-7075 particle where an individual BNNT was located. Figure 31 shows the individual BNNT, which was found using high magnification on the SEM. The diameter of the BNNT in Figure 31 appears to have a diameter that is within the manufacturer's specifications of 60 nm.

Figure 30. BNNT location on Al-7075 particle

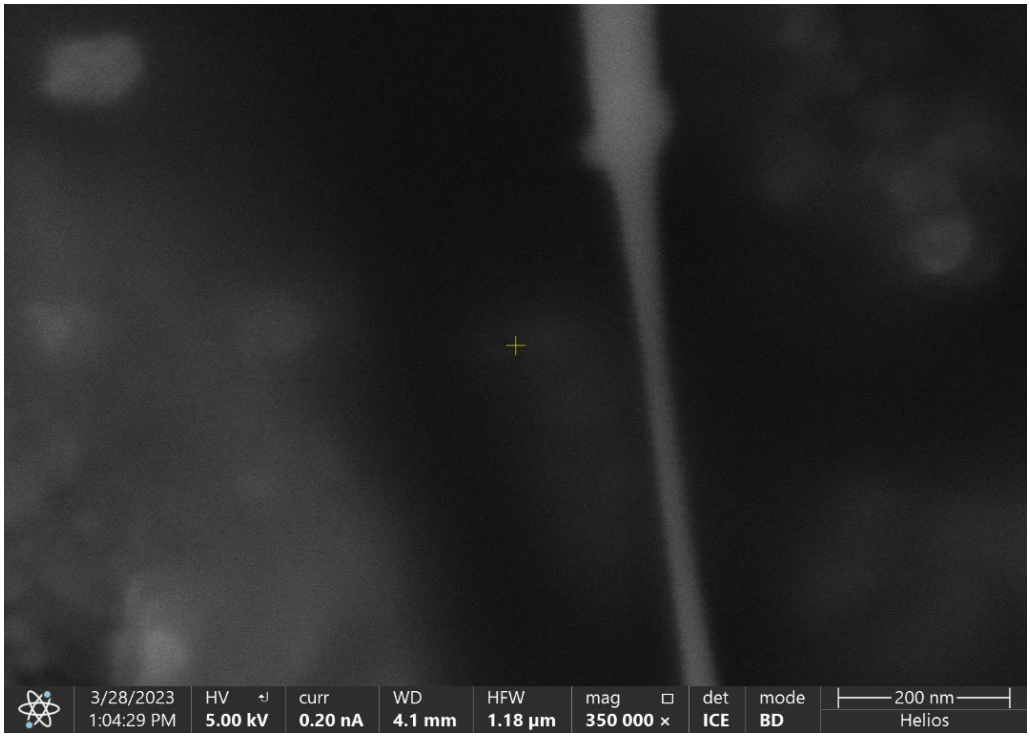

Figure 31. Individual BNNT located on Al-7075 particle as seen in Figure 30

The powder composition seems to be very well and evenly distributed, which we can conclude that the HEBM parameters that were used, and discussed in Chapter III, did a successful job with their intention of distributing the ceramics and maintaining the Al-7075 morphology with the MMC.

B. COLD SPRAY SAMPLE CHARACTERIZATION

1. Visual Inspection

After every sample was cold sprayed, a visual inspection was performed. Visual inspections looked for uniformity, porosity, and thickness, as well as any other details that stood out. Figure 32 shows the four graded coating compositions. The coatings that had a lower vol.% of alumina on the top layer appear to be slightly darker in color. All coatings appear very well distributed, with no raised edges, which can occur along the path of the deposition nozzle during coating application. No distinguishable visual difference in porosity was observed in any of the coatings post spraying. Though not always desirable, the coatings all appeared to be very thin in nature. The difference in thickness of the different coatings was not able to be determined from a post spray visual inspection.

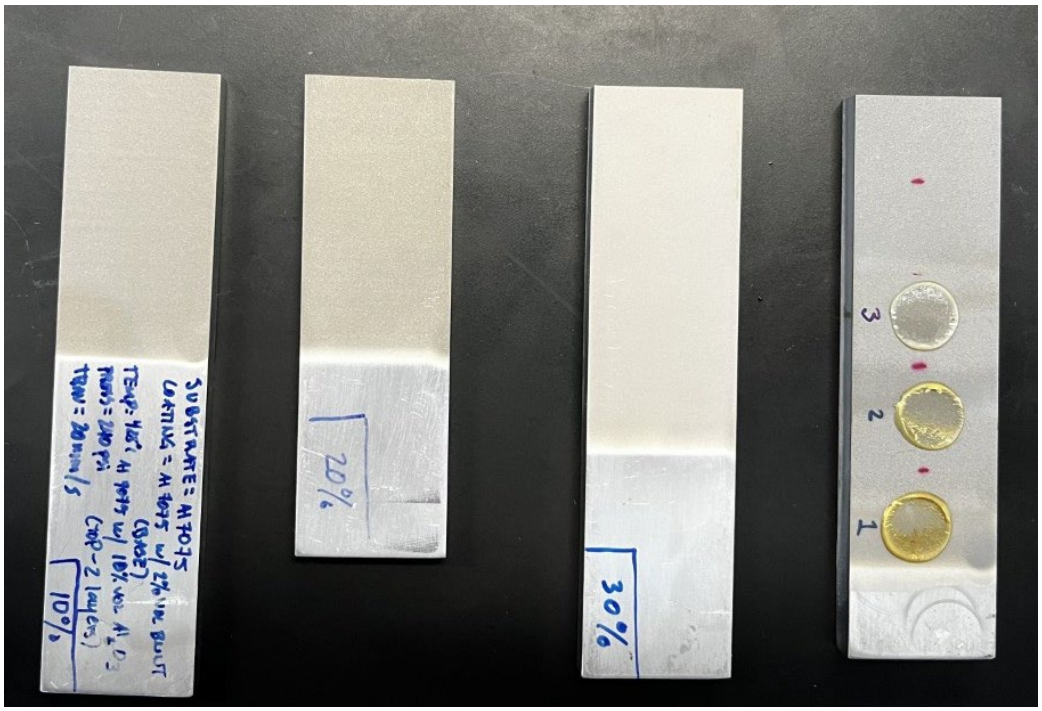

Figure 32. Cold spray compositions. Left to right: 10vol.% Al2O3 with Al-7075, 20vol.% Al2O3 with Al-7075, 30vol.% Al2O3 with Al-7075, 30vol.% Al2O3 with Al-7075 (middle coating layer composed of 1 vol.% BNNT, 10 vol.% Al2O3. 89 vol.% Al-7075. Note, all coating base layers are 2 vol.% BNNT with Al-7075

2. Optical Microscopy

Optical microscopy was performed on all samples by taking screen shots of live images on the optical microscope, which was discussed in Chapter III. The optical microscope imagery confirmed that the coating thickness was much less than desired, which appeared to be between 10 and 20 μm. It was decided that the average coating thickness would be determined during imaging in the SEM where imbedded software features allow for measurements of the digital image. The optical microscope images were used to ensure that the polishing of the cross-sectioned samples was adequate prior to chemical etching, and that the visible scratches on the surface was at a minimum to ensure accurate characterization once the samples were mounted in epoxy and consequently examined in the SEM. Optical imagery from each cold spray composition can be seen in Figure 33.

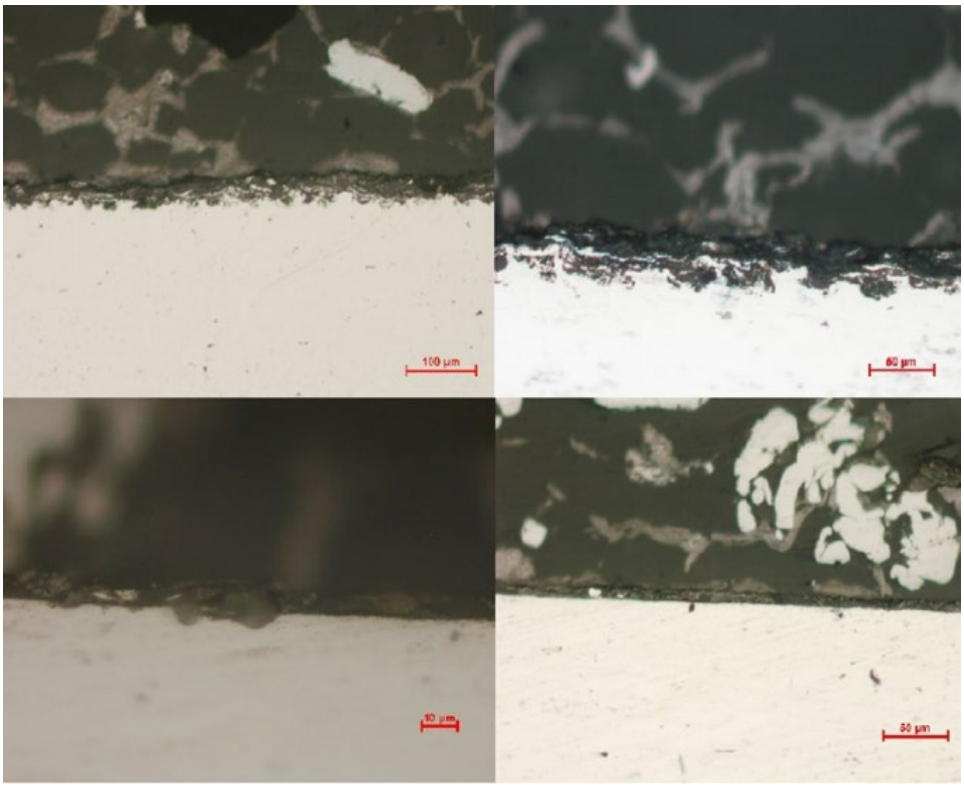

Figure 33. Optical microscope images of all four compositions. Starting top left clockwise: 10vol.% Al2O3 with Al-7075, 20vol.% Al2O3 with Al-7075, 30vol.% Al2O3 with Al-7075, 30vol.% Al2O3 with Al-7075 (middle coating layer composed of 1 vol.% BNNT, 10 vol.% Al2O3. 89 vol.% Al-7075. Note, all coating base layers are 2 vol.% BNNT with Al-7075

The optical imagery did show that the general microstructure and visible splat structure of all cold spray coatings was similar in appearance and morphology, leading to the conclusion that the cold spray application process for each coating was consistent.

3. SEM Microstructural Characterization

Due to the relatively thin thickness of the cold spray coatings, SEM imagery was chosen to measure more accurately the average thickness of the individual coatings. The average coating thicknesses are recorded in Table 10. The thickness measurements were obtained during SEM imagery by measuring the cross-sectioned samples, which had been polished and subsequently chemically etched. Figure 34 details a sample SEM image from which thickness measurements were obtained. The thickest average coating, as seen in

Table 10, is the composition that contains 10 vol.% alumina, followed by the compositions containing 20 vol.%, 30 vol.%, and the functionally graded composition, respectively. As the volume percentages of the ceramic reinforcements increases, the coating thickness decreases. The most noticeable jump in average coating thickness occurs between the 10 vol.% and 20 vol.% alumina compositions. The higher vol.% of alumina within the Al-7075-Al_2O_3 compositions seem to be providing compaction of the coating when sprayed onto the Al-7075 substrate. This is possibly due to what was noticed by Irissou et al. [21] during their study of Al-Al_2O_3 cold spray coating formation and properties. It was determined that the inclusion of hard ceramic Al_2O_3 reinforcements on spherical Al particles primarily play a role of peening and roughing the layers of coating during deposition [21]. It is this peening effect that the alumina provides during deposition that will compact the coating during cold spray application. With a higher vol.% of alumina in the composition, you will have an increased peening effect, thus decreasing the overall thickness of the applied coating.

Table 10. Average coating thickness

Top Layer Composition	Mid-Layer Composition	Bottom Layer Composition	Average Thickness (µm)
90 vol. % Al-7075 / 10 vol. % Alumina	N/A	98 vol. % Al-7075 / 2 vol. % BNNT	**13.66**
80 vol. % Al-7075 / 20 vol. % Alumina	N/A	98 vol. % Al-7075 / 2 vol. % BNNT	**9.94**
70 vol. % Al-7075 / 30 vol. % Alumina	N/A	98 vol. % Al-7075 / 2 vol. % BNNT	**9.33**
70 vol. % Al-7075 / 30 vol. % Alumina	89 vol. % Al-7075 / 10 vol.% Alumina / 1 vol. % BNNT	98 vol. % Al-7075 / 2 vol. % BNNT	**7.99**

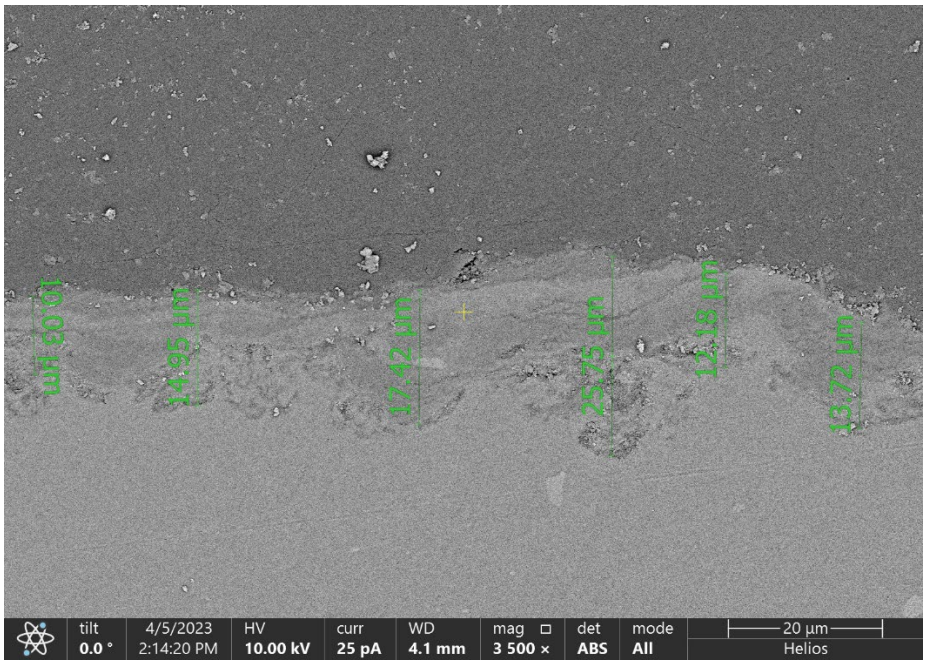

Figure 34. SEM thickness measurements of AL-7075 with 10 vol.% alumina

All coating compositions were inspected under the SEM to examine the microstructure, determine the presence of the reinforcing ceramics, observe the proper dispersion of the reinforcing ceramics, and examine the splat boundaries. These splat boundaries are formed during the cold spray process. When the particles strike the substrate, they flatten and form into think layers that adhere to the substrate and to each other. The interface of the splat boundaries is the location where reinforcing particles will be found, especially when examining under the SEM. This is due to the fact that when the powders are processed during the HEBM process, the reinforcing ceramics adhere to the surface of the Al-7075 particles. Then once the powder is sprayed and the particles are plastically deformed upon impact, the reinforcing material is distributed throughout the splat boundaries proportionate to the vol.% in which the Al-7075 powder prior to spraying. Figure 35 shows an SEM where these splay boundaries are visible within the coating. Some of these splat boundaries have been overlayed in red to make visualization easier. The splat boundaries that have not be overlayed in red can be identified by the black lines or voids found in the image.

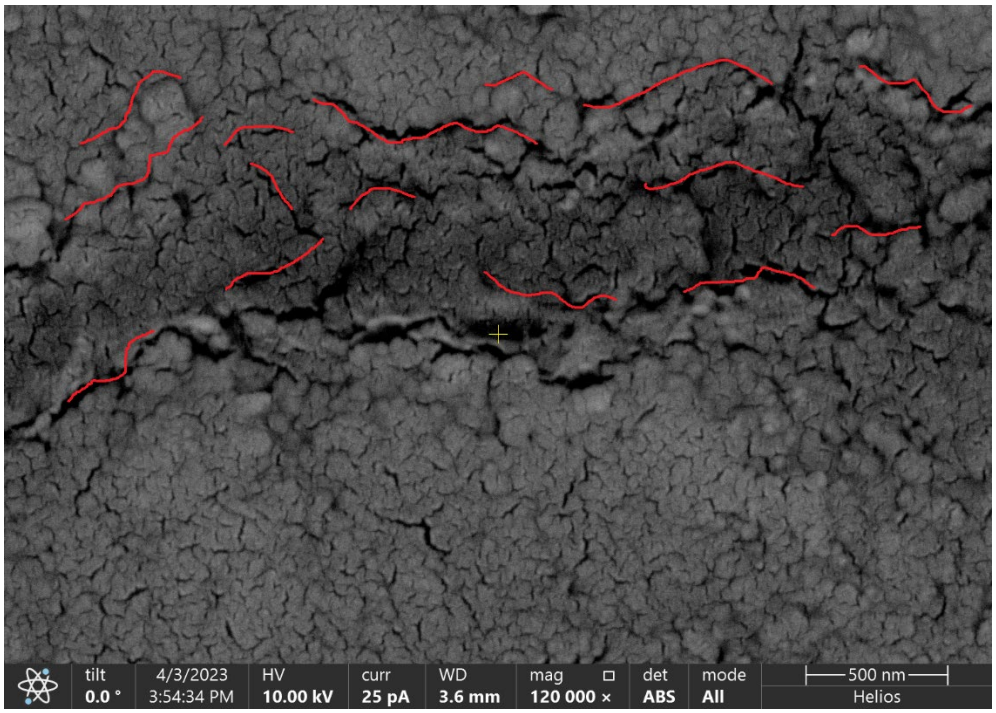

Figure 35. SEM image of splat boundaries found within the coating

Figure 36 shows a lower magnification of the same coating (top layer = 30vol.% alumina, 70vol.% Al-7075, middle layer = 1vol.% BNNT, 10vol.% alumina, 89vol.% Al-7075, bottom layer = 2vol.% BNNT, 98vol.% Al-7075).

Figure 36. SEM image of coating at lower magnification

In Figure 36, you can see the coating boundary layers where different compositions were used to effectively grade the overall coating to the substrate. This can be seen in the difference in the contrast of the coating as seen in the SEM image (the lightest shading as seen on the bottom portion of the image is the Al-7075 substrate).

One of the important concepts of this study was determining the effects that graded layers of cold spraying have on the coating's mechanical properties. SEM imagery was used to confirm that the layers were consistent in nature, that is that they were visibly present and not deformed after the coating application process. For the remainder of this study the coatings and their various layered compositions will be discussed as coating 1, 2, 3, and 4. The coatings and their respective layered compositions are detailed in Table 11. The SEM imaging on coatings 1, 2, and 3 determined that the base layer containing BNNTs was present and uniform throughout the coating, as seen in Figure 37. Figure 37 shows the graded coating layering of the base layer of BNNTs and the top coating containing Al-7075 with 30vol.% alumina. This general microstructure of the graded layers remained consistent for coating 1, 2, and 3. However, the thickness of the BNNT layers for coatings

1, 2, and 3 ranged from 1µm to 3µm, which is relatively thin for cold spray coatings. These measurements were compared to a control coating which contained 98vol.% Al-7075 and 2vol.% BNNT. The control coating was cross-sectioned, mounted, and polished with the same procedures as previously discussed. It was found that the average thickness of the BNNT control coating ranged 6-10µm. The result of applying an additional layer over the Al-7075/BNNT base layer resulted in approximately 50–80% compaction of the base coating, as measured in the vertical direction. Figure 38 shows an SEM image with measurements of BNNT control coating. The compaction of the BNNT layer in the graded coatings is possibly due to the peening effect during the application of the higher vol.% of ceramic reinforcements within the top coating, as previously discussed in this chapter. Other factors that possibly affected the thickness of the coatings examined in this study are discussed later in this chapter.

Table 11. Coating compositions

Coating Number	Top Layer Composition	Mid-Layer Composition	Bottom Layer Composition
1	90 vol. % Al-7075 / 10 vol. % Alumina	N/A	98 vol. % Al-7075 / 2 vol. % BNNT
2	80 vol. % Al-7075 / 20 vol. % Alumina	N/A	98 vol. % Al-7075 / 2 vol. % BNNT
3	70 vol. % Al-7075 / 30 vol. % Alumina	N/A	98 vol. % Al-7075 / 2 vol. % BNNT
4	70 vol. % Al-7075 / 30 vol. % Alumina	89 vol. % Al-7075 / 10 vol.% Alumina / 1 vol. % BNNT	98 vol. % Al-7075 / 2 vol. % BNNT

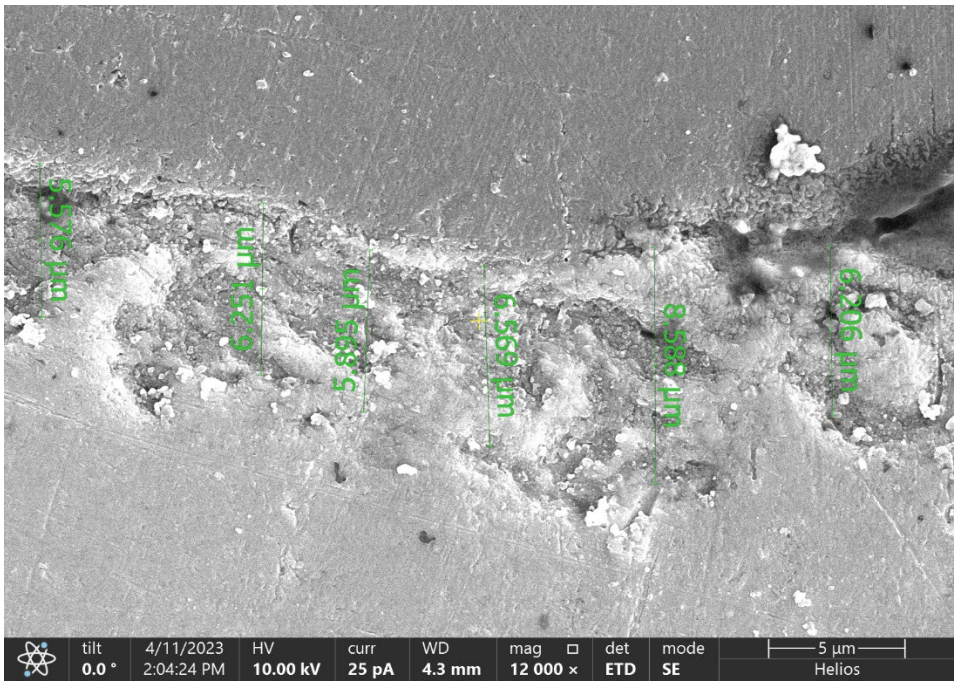

Figure 37. SEM image of Al-7075/BNNT control coating

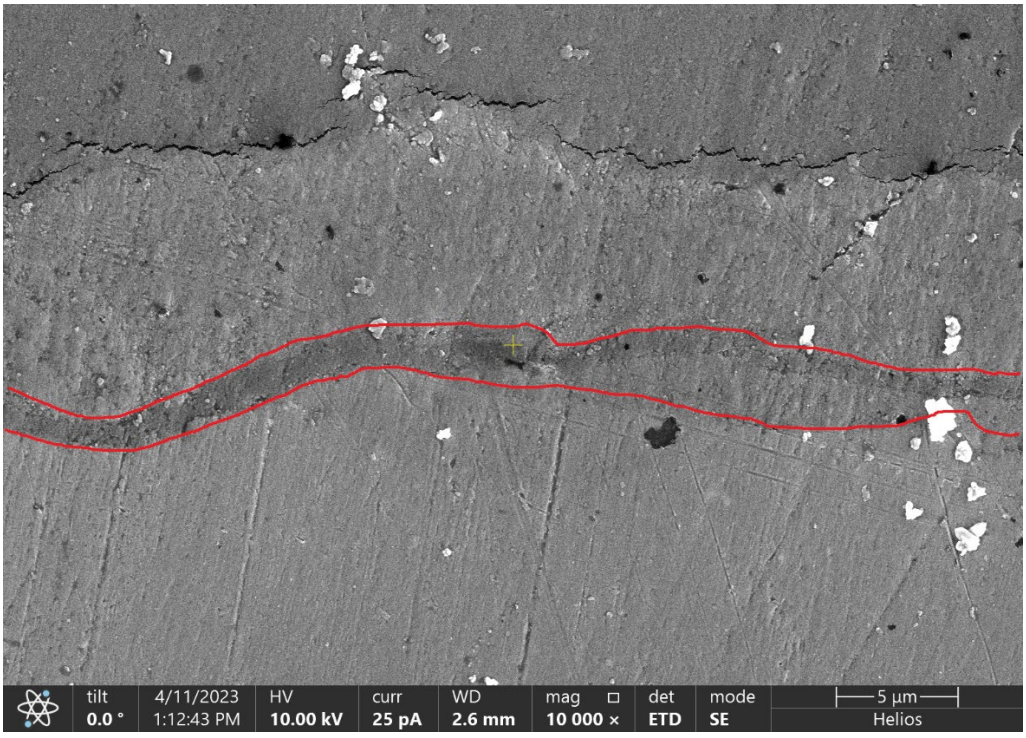

Figure 38. BNNT base layer, as seen in red, of coating 3

Figure 39 details the composition of the graded layers as seen in Table 11, the numbers 1, 2, and 3 correspond the top, middle, and bottom layers, respectively. The red boundary lines indicate approximately where the different layers interface with one another.

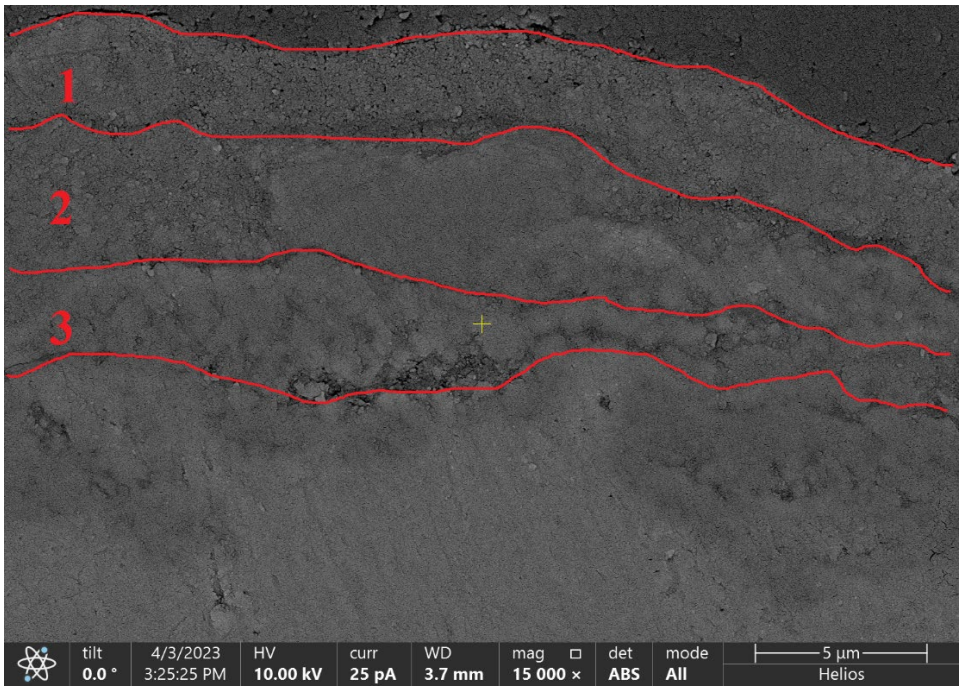

Figure 39. Compositional layering of coating 4

As discussed earlier in this chapter, SEM imaging was used to verify the presence of the reinforcing ceramics, specifically in and around the splat boundaries of the coatings. The coating compositions that contained alumina were found to be very evenly dispersed within the splat boundaries. Figure 40 shows an SEM image taken on a cross-sectioned sample from coating 1. The Everhart-Thornley detector (ETD) was used to obtain the image in Figure 40, especially because the charging of the alumina reinforcements can be more readily identified in the boundary layer of the compositions interface. Figure 41 shows alumina particles within the splat boundary of coating 3. This image not only details the flattening effect that occurs to the particles in the plat boundary, but also shows an individual alumina particle that has bridged the gap between the splat boundaries. It should

be noted that during examination of coatings 1, 2, and 3, the distribution of alumina within the coating was consistent with the coating's respective vol.%. The images shown are for reference as it applies to all coatings containing alumina as a reinforcement particle.

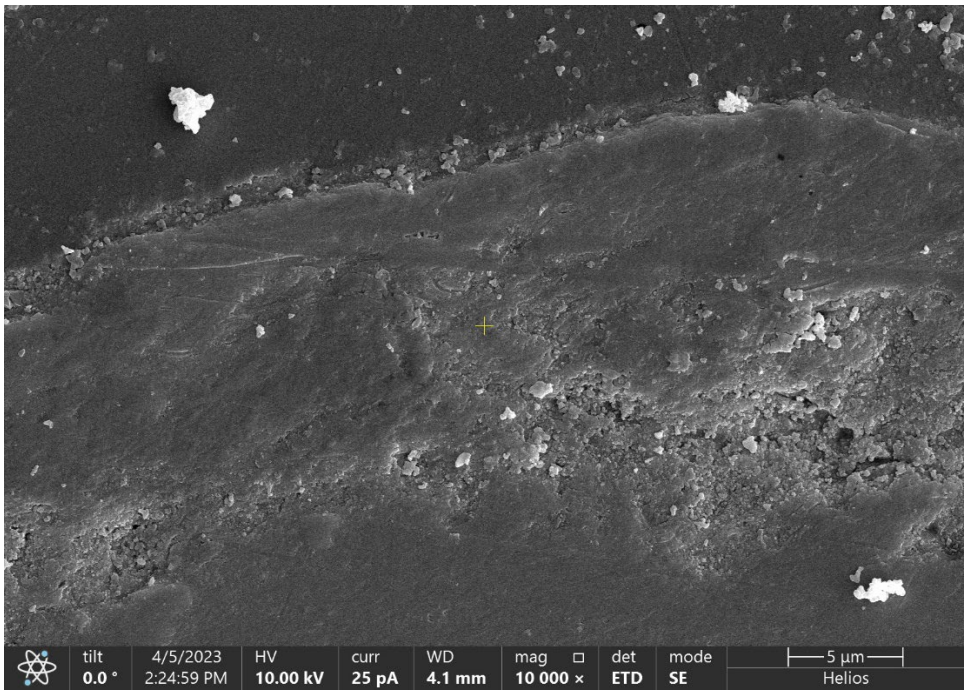

Figure 40. SEM image of alumina at coating interface of coating 1

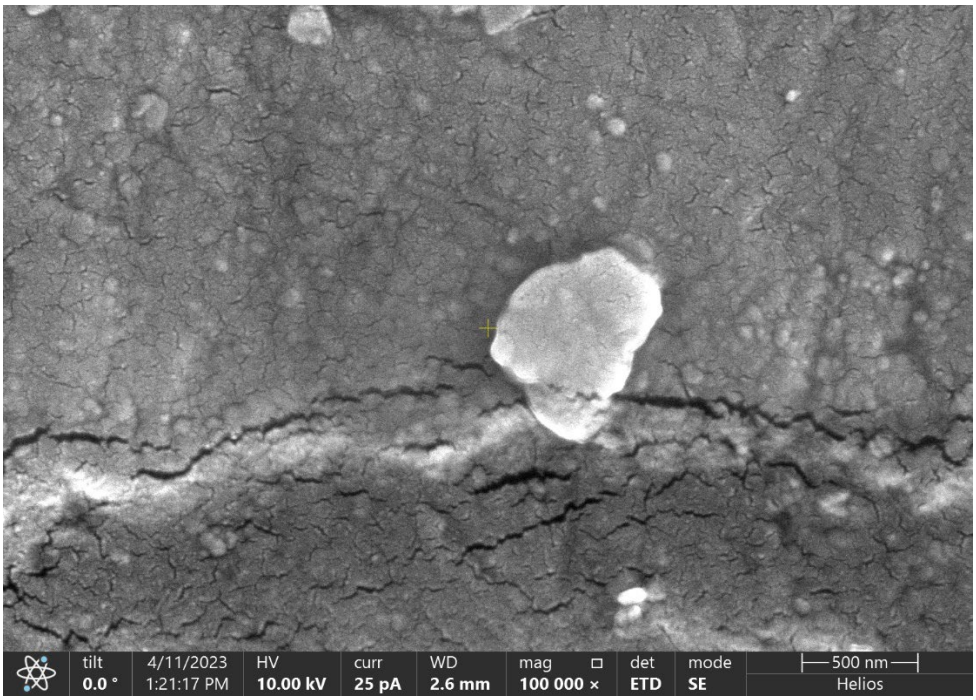

Figure 41. SEM image of alumina within splat boundary interface with individual alumina particle bridging splat boundary of coating 3

Figures 42 and 43 show a BNNT located in splat boundaries of coatings 1 and 4, respectively. Figure 42 was taken at a higher magnification to better determine the morphology of the BNNT particle, which appeared to be imbedded into the surrounding composition. Figure 43, which was taken on coating 4, shows what appears to be BNNTs bridging the splat boundary gap. This image was taken near to the interface location of the bottom and middle layers of coating 4, which contained 1 vol.% and 2 vol.% of BNNTs, respectively.

Figure 42. SEM image of individual BNNT located in coating 1

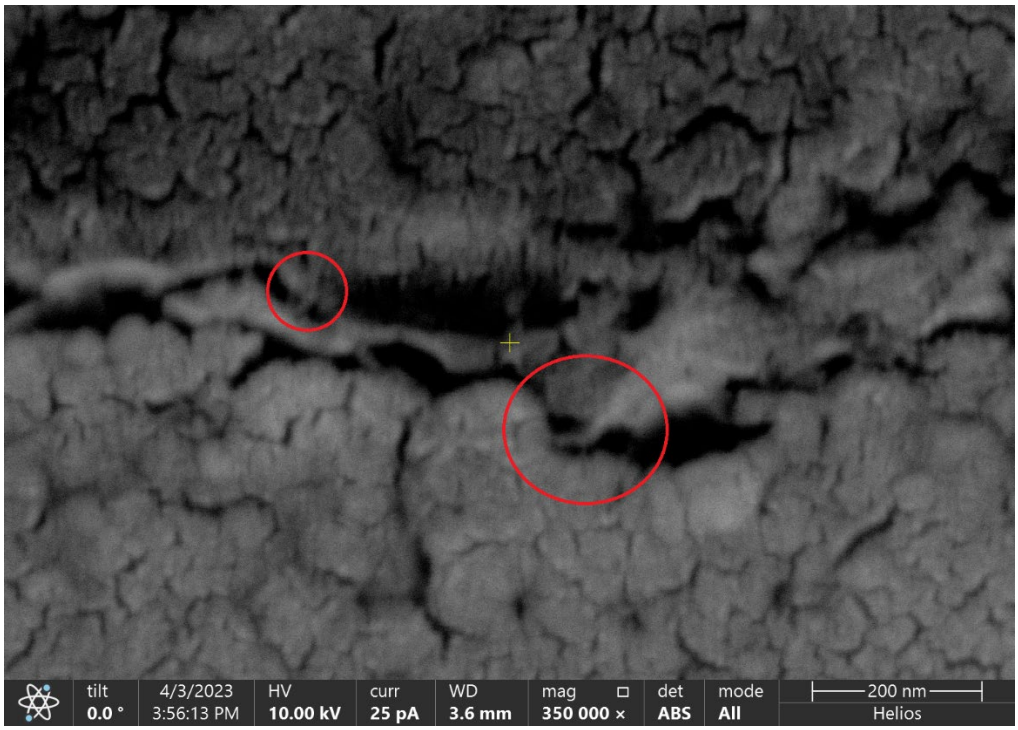

Figure 43. SEM image of possible BNNTs bridging splat boundary of coating 4, as circled in red (350kX magnification)

SEM imagery of the cross sectioned samples showed that the reinforcing ceramics that were used in the various powder compositions were evenly distributed and were consistently found in and around the splat boundaries and compositional layer interfaces.

4. SEM Top-Down Imagery of Top Layer Compositions of Cold Spray Coatings

After the final top layer was applied to all cold spray coatings a visual inspection was performed to note any differences in the coating structure. Since all top coating layers were relatively similar in composition, apart from the differences in alumina vol.%, the visual inspection results were inconclusive, therefore top-down SEM imagery was performed. The only significant difference that was initially observed during the SEM top-down imagery was the presence of spherical craters imbedded into the top layer of the coatings. Initially it was thought that the coatings containing higher vol.% of alumina had fewer noticeable craters, however after further analysis using ImageJ software it was determined that the number of craters on the different compositions of top layer coating was approximately withing 5% of one another. Figure 44 shows the top-down SEM imagery of coatings 1, 2, and 3. It should be noted that top-down imagery of coating 4 was omitted due to it having the same Al-7075/alumina composition of coating 3.

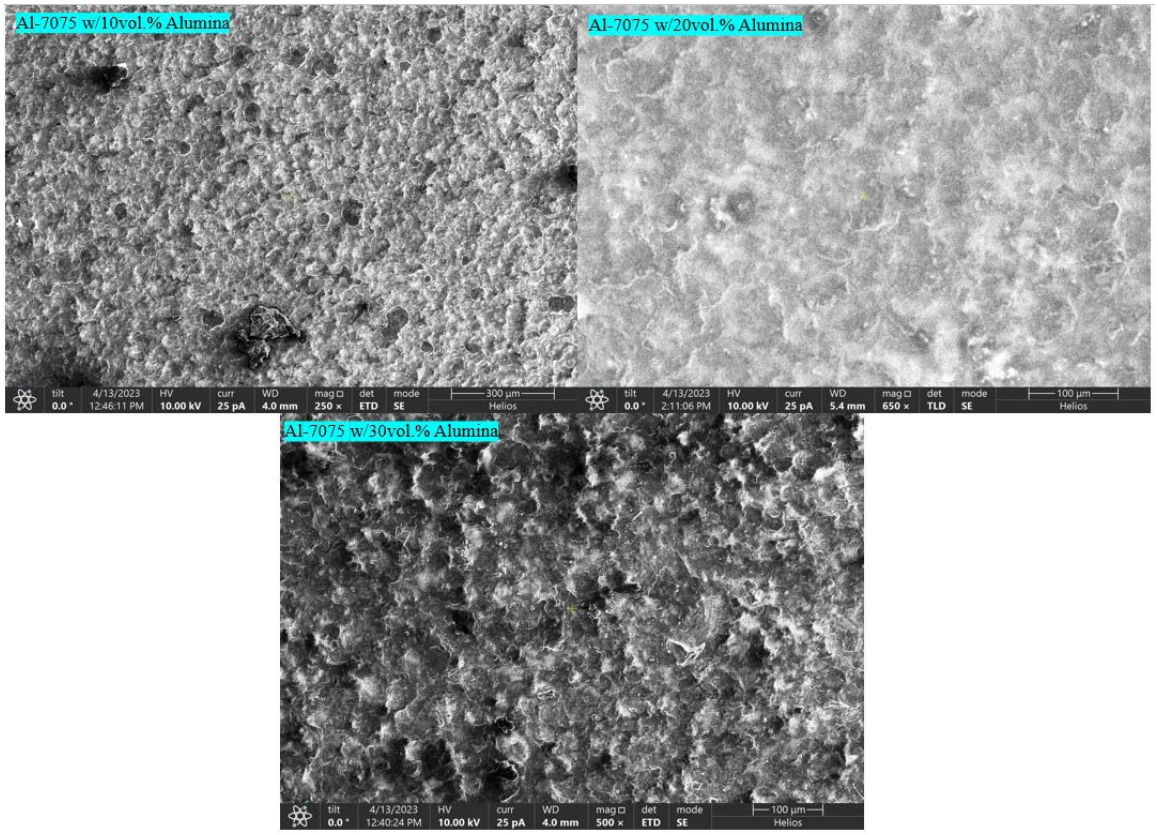

Figure 44. Top-down SEM images of top layer compositions of cold spray coatings

The general shape of the craters that were observed in the top-down imagery were consistent with that of a sphere. The diameter of the craters ranged from approximately 12µm to 60µm. This size distribution is consistent with the size distribution of the as-received Al-7075 spherical powder used in this study. It is possible that during the cold spray process, some of the Al-7075 particles did not reach the critical velocity required to adhere to the substrate and/or built up coating, which would mean that the Al-7075 particles impacted the coating without enough kinetic energy to deform and cause adherence to the coating. Effectively some Al-7075 particles did not reach critical velocity and bounced off the coating surface leaving noticeable spherical craters. Figure 45 details the dimensions of a such a crater found during top-down SEM imaging of coating 1.

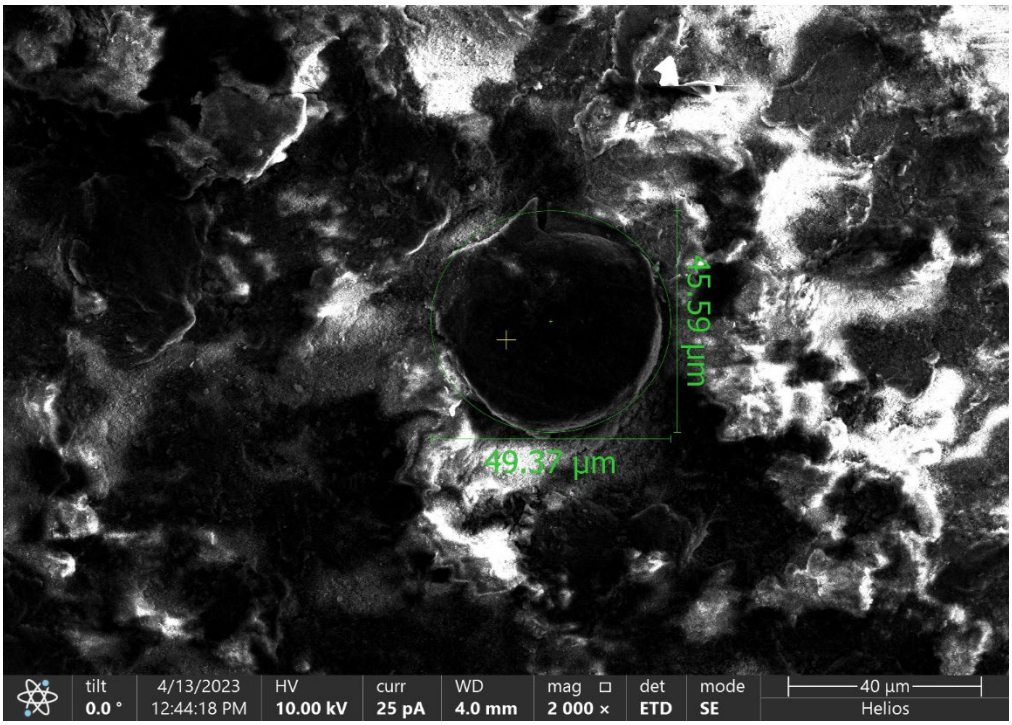

Figure 45. Top-down SEM image of impact crater on coating 1

C. ADHESION

Adhesion tests were performed on all coating compositions, to include adhesion tests on control coatings. Figure 46 shows a cold sprayed sample post-adhesion test. The graded cold spray coating and their respective average adhesion strengths are detailed in Table 12. The control coatings and their respective average adhesion strength are detailed in Table 13. Figure 47 shows the average adhesion strength of each of these coatings at the time of fracture. The black bars in Figure 47 represent one standard deviation from the mean adhesion strength given that coating's composition.

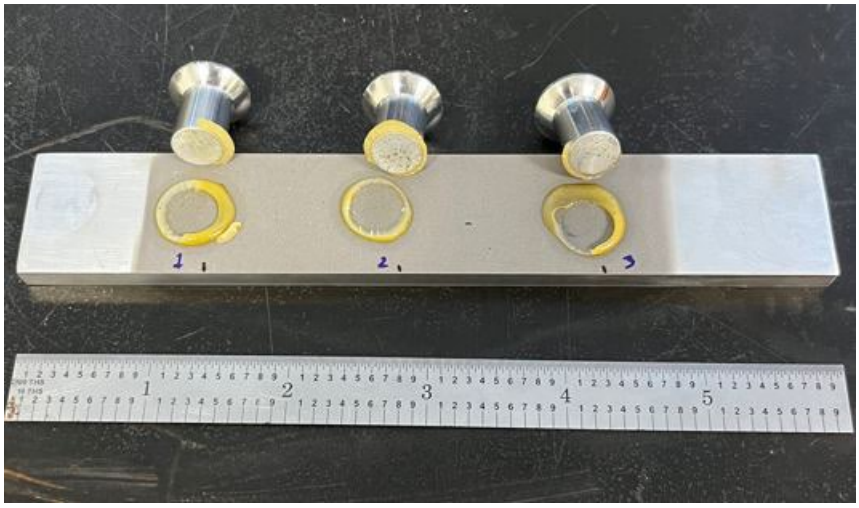

Figure 46. Adhesion test post failure for coating 3

Table 12. Graded cold spray compositions and adhesion strength

Graded Coating Number	Top Layer Composition	Mid-Layer Composition	Bottom Layer Composition	Average Adhesion Strength (MPa)
1	90 vol. % Al-7075 / 10 vol. % Alumina	N/A	98 vol. % Al-7075 / 2 vol. % BNNT	**43.15**
2	80 vol. % Al-7075 / 20 vol. % Alumina	N/A	98 vol. % Al-7075 / 2 vol. % BNNT	**44.25**
3	70 vol. % Al-7075 / 30 vol. % Alumina	N/A	98 vol. % Al-7075 / 2 vol. % BNNT	**44.04**
4	70 vol. % Al-7075 / 30 vol. % Alumina	89 vol. % Al-7075 / 10 vol.% Alumina / 1 vol. % BNNT	98 vol. % Al-7075 / 2 vol. % BNNT	**51.58**

Table 13. Control cold spray compositions and adhesion strength

Control Number	Top Layer Composition	Mid-Layer Composition	Bottom Layer Composition	Average Adhesion Strength (MPa)
1	Al-7075 100 vol.%	N/A	N/A	**44.63**
2	98 vol.% Al-7075 / 2 vol.% BNNT	N/A	N/A	**27.68**
3	90 vol.% Al-7075 / 10 vol.% Alumina	N/A	N/A	**55.77**
4	80 vol.% Al-7075 / 20 vol.% Alumina	N/A	N/A	**59.14**
5	70 vol.% Al-7075 / 30 vol.% Alumina	N/A	N/A	**53.66**

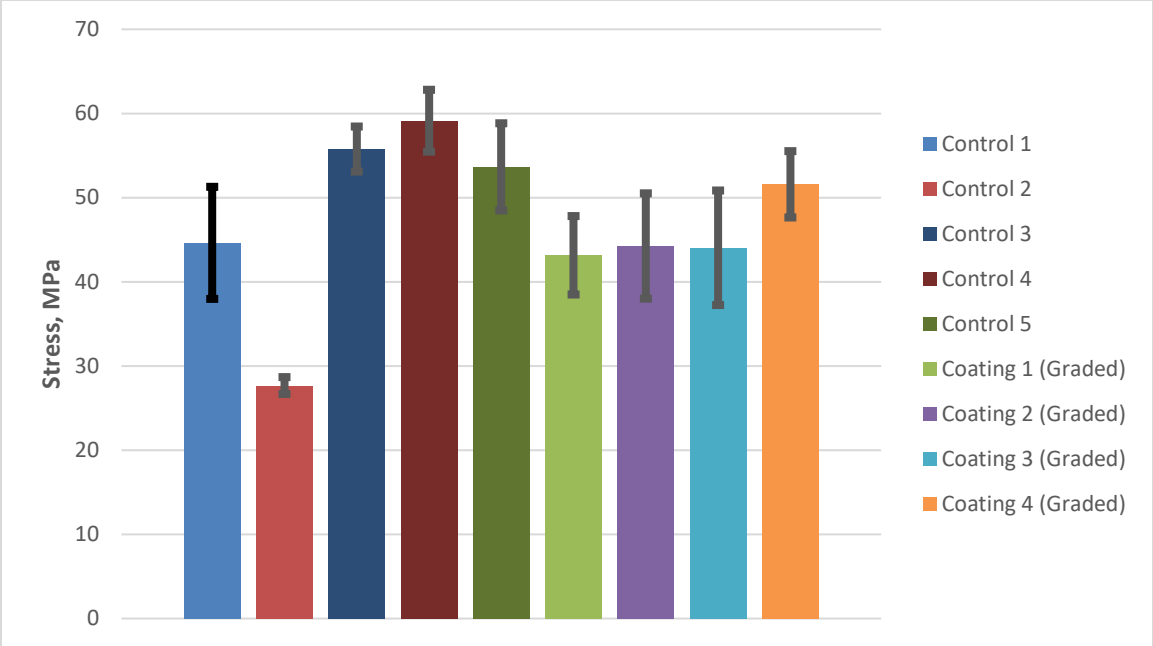

Figure 47. Adhesion results

The coating that had the highest adhesion strength was from control 4, the coating containing 80 vol.% Al-7075 and 20 vol.% alumina. Control coatings 3, 4, and 5 all had average adhesion strength's greater than that of any other coating tested. The highest of the graded cold spray coatings was graded coating 4, and although graded coatings 1, 2, and 3 were within 0.89 MPa of each other's adhesion strength, the lowest of the three was graded coating 1, which contained 10 vol.% alumina. The lowest adhesion strength of all coatings tested was control 2, which contained Al-7075 with 2 vol.% BNNTs.

The adhesions tests show conclusively that coatings containing alumina yield higher adhesion strength compared to those that contain BNNTs. However, the average adhesion strength of graded coatings 1, 2, and 3, which was 43.81 MPa, was a 1.83% decrease in strength from the average adhesion strength of the coating containing 100 vol.% Al-7075 (control 1). The control coating 3, 4, and 5, which respectively contained 10, 20, and 30 vol.% of alumina had on average a 12.37 MPa higher adhesion strength than the graded coatings which contained the same vol.% of alumina on for their top layer coating. These results further support the conclusion that the base layer coatings containing BNNTs negatively affect the adhesion strength performance.

Adhesion failure can occur in three different modes. The first being failure of the glue at the dolly interface, the second being the coating at the substrate interface (delamination), and the third being failure within the coating itself (cohesive failure). All adhesion tests conducted in this study either failed completely cohesively or cohesively with partial delamination. The tests conducted on all graded cold spray coatings (graded coatings 1, 2, 3, and 4) were cohesive failures, which was confirmed by SEM imaging. Of the control samples, control 1 and 2 failed both through delamination and cohesively. Control 3, 4, and 5 failed completely cohesively. With cohesion being the primary adhesion failure mode for all cold spray samples in this study, it suggests that the bonding between the particles, in the case of the control samples, was strongest at the substrate interface when compared to that of the bonding between the particles within the coating itself. As far as the graded layers are concerned, it was initially unclear whether the bonding failed within the specific layered composition (i.e., the top, middle, or bottom layer), or at the layered compositional interfaces. SEM imaging was used to determine the presence of the reinforcing ceramics within the failure zone to conclude if the failure occurred within the compositional layer or at the layer interface of the graded cold spray coatings (graded coatings 1, 2, 3, and 4).

To ensure that the coatings remained intact at the conclusion of testing, it was decided that top-down SEM imaging would yield better results as opposed cross-sectional imaging. Figure 48 shows an SEM top-down image of coating 1 within the adhesion failure zone. Even at this low magnification distinct ridges, indicative of a ductile failure are visible. Also visible is the characteristic charging due to alumina which can be seen circled in red in Figure 48.

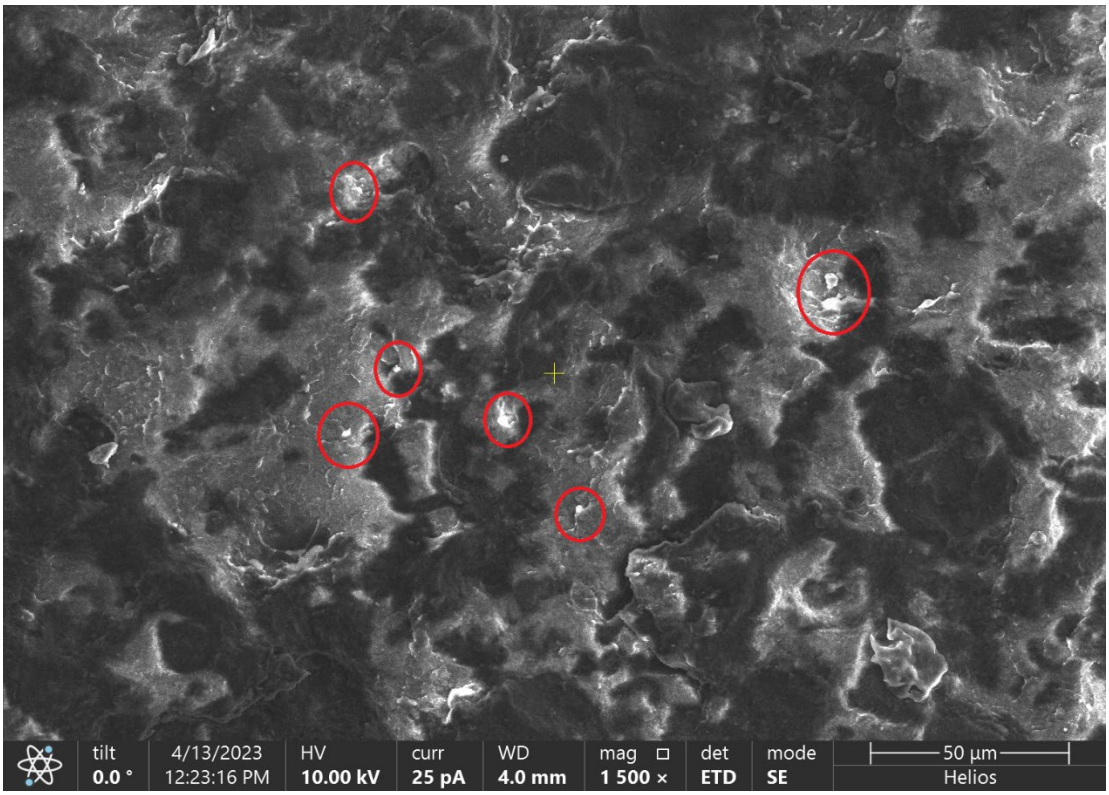

Figure 48. Top-down SEM image of coating 1 in failure zone

Figure 49, which is a top-down SEM image of graded coating 2 within its adhesion failure zone, has what appears to be slightly distorted Al-7075 particles (circled in yellow) which still have remnants of alumina bonded to them. Also visible in Figure 49 are the splat boundaries, which appear to have been broken away and now have a visual likeness to contours on a map (circled in red). These characteristics were consistent with all the graded coatings adhesion failure zones.

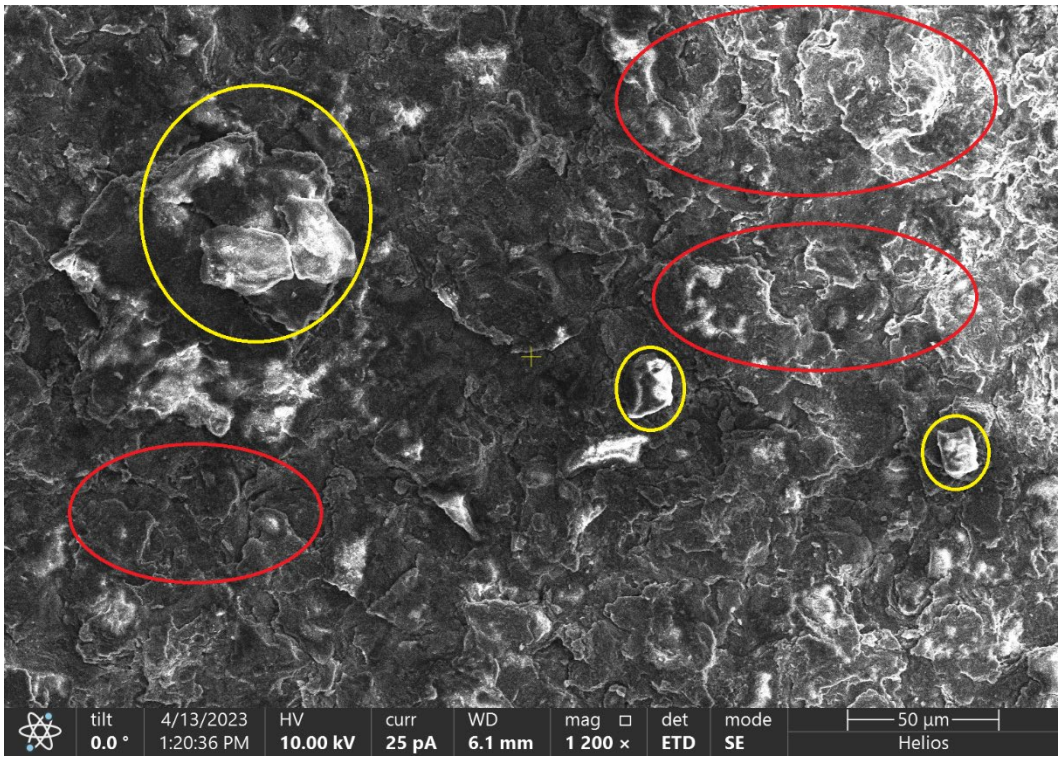

Figure 49. Top-down SEM of coating 2 in failure zone

Determining the presence of BNNTs proved to be challenging. The presence of BNNTs within the failure would indicate that the cohesive failure occurred at or near the compositional interface and not within the compositional layer itself. Figure 50 shows what appears to be an individual BNNT (located center image, circled in red) and a possible chopped BNNT (located top-center image, circled in red). The presence of BNNTs were found while conducting top-down SEM imaging for graded coatings 1, 2, and 3. This allows for the conclusion that the adhesion failure for these three coatings occurred not within the compositional layer, but rather at the compositional layer interface.

Figure 50. Top-down SEM image of BNNTs located in coating 2

Graded coating 4, which had an average adhesion strength of 51.58 MPa, was unique when compared to graded coatings 1, 2, and 3 in the sense that it has the inclusion of a middle-graded layer. This layer which includes Al-7075, alumina, and BNNTs (vol.% detailed in Table 12), is possibly why the adhesion strength of graded coating 4 was 7.76 MPa greater than the average of graded coating 1, 2, and 3. During top-down SEM imaging of the adhesion failure zone of graded coating 4, the same approach was taken to locate ceramic reinforcements in an attempt to determine the possible location of cohesive failure within the coating. No images obtained from the top-down SEM imagery from graded coating 4 contained any discernible BNNTs. However, the presence of alumina was very prevalent with the coating failure zone, as seen in Figure 51. The two possible conclusions for coating 4 are that the coating failed cohesively in within one of the layered compositions or failed between the top and mid-layer compositions. The presence of the alumina in the middle compositional layer might be the contributing factor as to why graded coating 4

displayed consistently higher adhesion strength as compared to the coating that had only two graded layers.

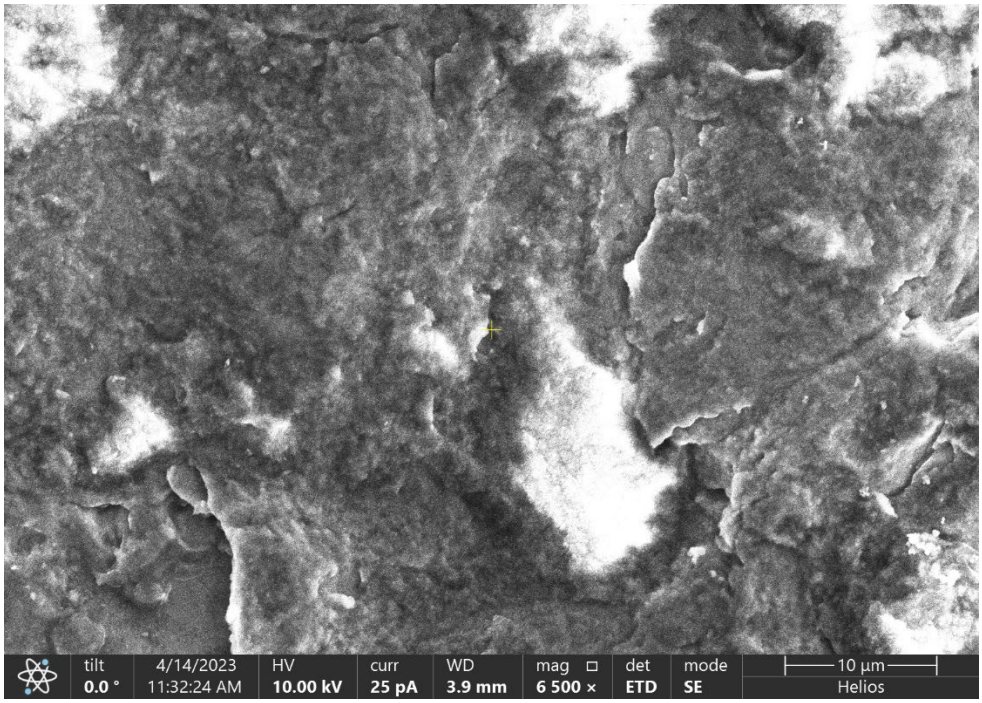

Figure 51. Top-down SEM image within adhesion failure zone of coating 4

After the examination of the test results and top-down imagery from the adhesion tests it does appear that the layers containing BNNTs negatively affected the potential adhesion strength of the cold spray coatings. The increase of adhesion strength when a middle compositional layer is added, as seen from the adhesion test results for coating 4, is very promising, especially when taking into consideration that the failure occurred cohesively, which does not expose the substrate since the failure occurs with the coating itself. The end results for graded coatings 1, 2, 3, and 4 ranged between 43.15 MPa and 51.58 MPa, which is remarkable, especially when compared the 7.01 MPa average adhesion strength of polysiloxane coatings used for Naval vessels [43].

D. WEAR

Wear testing was conducted on graded coatings 1, 2, 3, and 4 (see Table 12). The data was compared to determine the effect that 10, 20, and 30 vol.% of alumina (the vol.% of alumina present in each of these coatings top layer composition) would contribute to the overall wear resistance of the coating. Graded coatings 1, 2 and 3 all had the same bottom layer cold spray composition (Al-7075 with 2 vol.% BNNT). The results from graded coating 4 showed the effect of an additional graded layer (i.e., the middle layer, refer to Table 12) to the overall wear resistance of the coating. As previously discussed in Chapter II, Section F, the introduction of alumina has been seen to increase the wear resistance of cold sprayed coatings significantly [30]. There is no literature to date on how graded layers of cold spray affect the overall wear resistance of the coating.

Graded coating 1, 2, 3, and 4 all underwent wear testing, and the respective masses of the samples were recorded before and after each test to determine the total mass loss. The average mass loss for each coating was tested and recorded in Figure 52. With regards to the graded coatings containing only two compositional layers (graded coatings 1, 2, and 3), it is quite clear that the mass loss decreased as the vol.% of alumina increased. Fernadez et al. [30] concluded that Al-Al_2O_3 coatings did not show increased wear resistant properties until the wt.% was at or above 20 wt.%, from which point the wear resistance would gradually increase until a wt.% of around 39 wt.% [30]. In this study, Al-7075 with 20.vol% and 30 vol.% alumina are the only compositions that have over 20 wt.% of alumina. The coatings containing 20 or 30 vol.% of alumina equate to 26 wt.% and 37 wt.% of alumina, respectively. The amount of alumina in graded coatings 2 and 3 could possibly be the reason why a decrease in mass loss was seen as compared to graded coating 1 whose wt.% of alumina was below 20 wt.% (13.51 wt.%). This same reasoning might also be applied to graded coating 4, whose middle layer had 10 vol.% of alumina, however, results remain inconclusive due to the wear depth reached during testing.

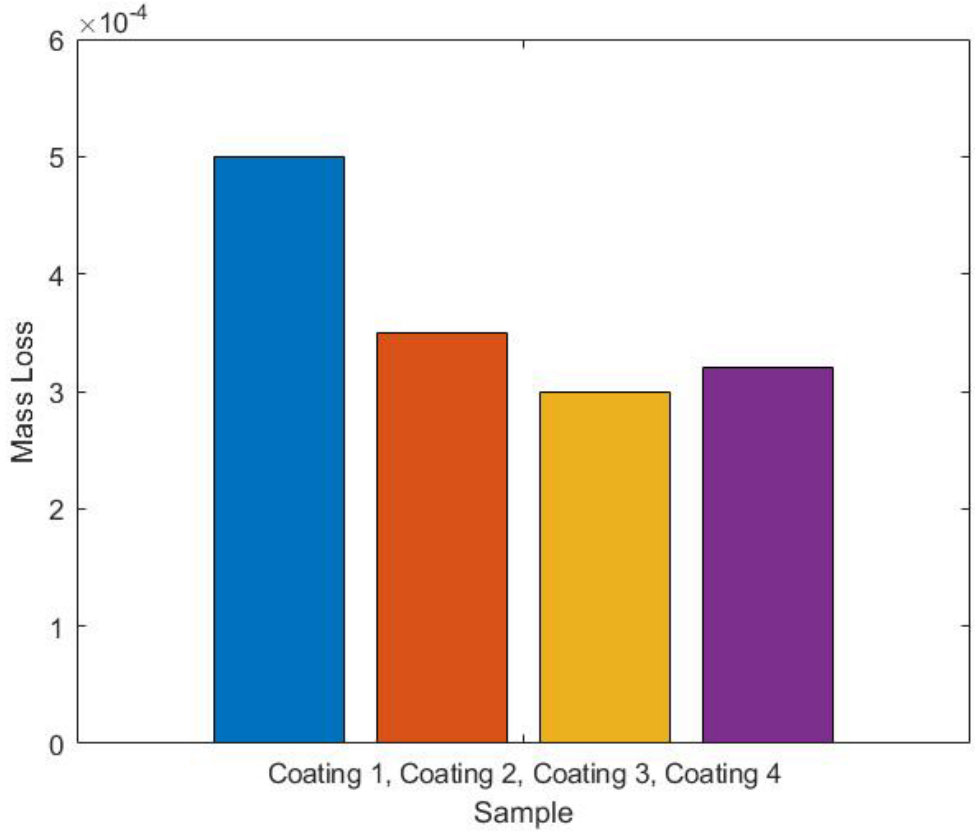

Figure 52. Average mass loss (grams) during wear testing

During wear testing, the coefficient of friction (COF) was recorded for each coating. The COF was recorded in real-time and can be seen plotted in Figure 53. The data acquired from the wear tester required further data manipulation due to the noisiness of the data collection. A moving mean was applied to the data that was received from the wear tester to make the data more readable. The data seen in Figure 53 is still noisy in nature, however, some insightful data can still be extracted. As seen in Figure 53, the initial COF recorded starts relatively high, then trends downward. This is because the wear tracks in the coating have not fully taken formation, leading to a rougher COF reading.

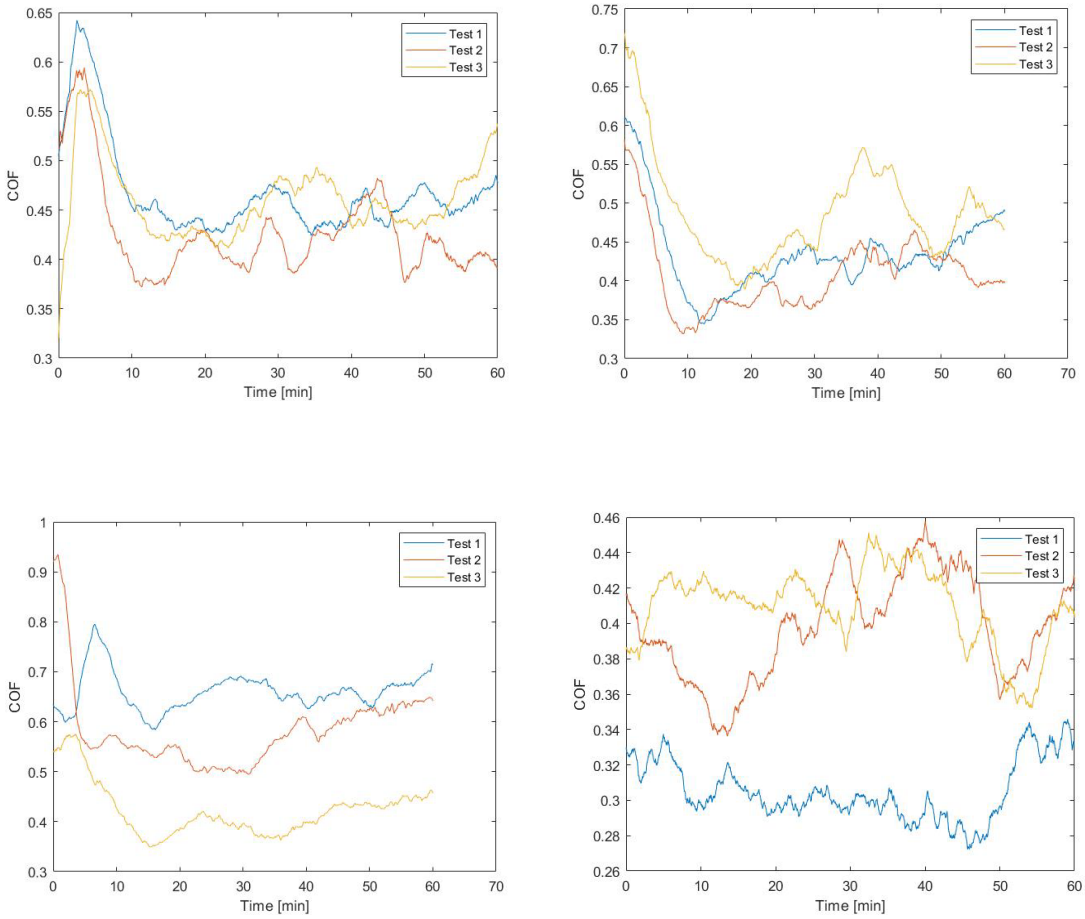

Figure 53. Coefficient of friction for coatings during wear testing. (Clockwise from top left: graded coating 1, graded coating 2, graded coating 4, graded coating 3)

The wear tester also recorded the depth of the wear track, which was taken in real-time. This data was also manipulated using the same procedure as described for the COF. Before each test was conducted, the depth recorder was zeroed, so any negative values recorded are effectively above the zero-depth mark. All plots for encoder depths are displayed in Figure 54 below.

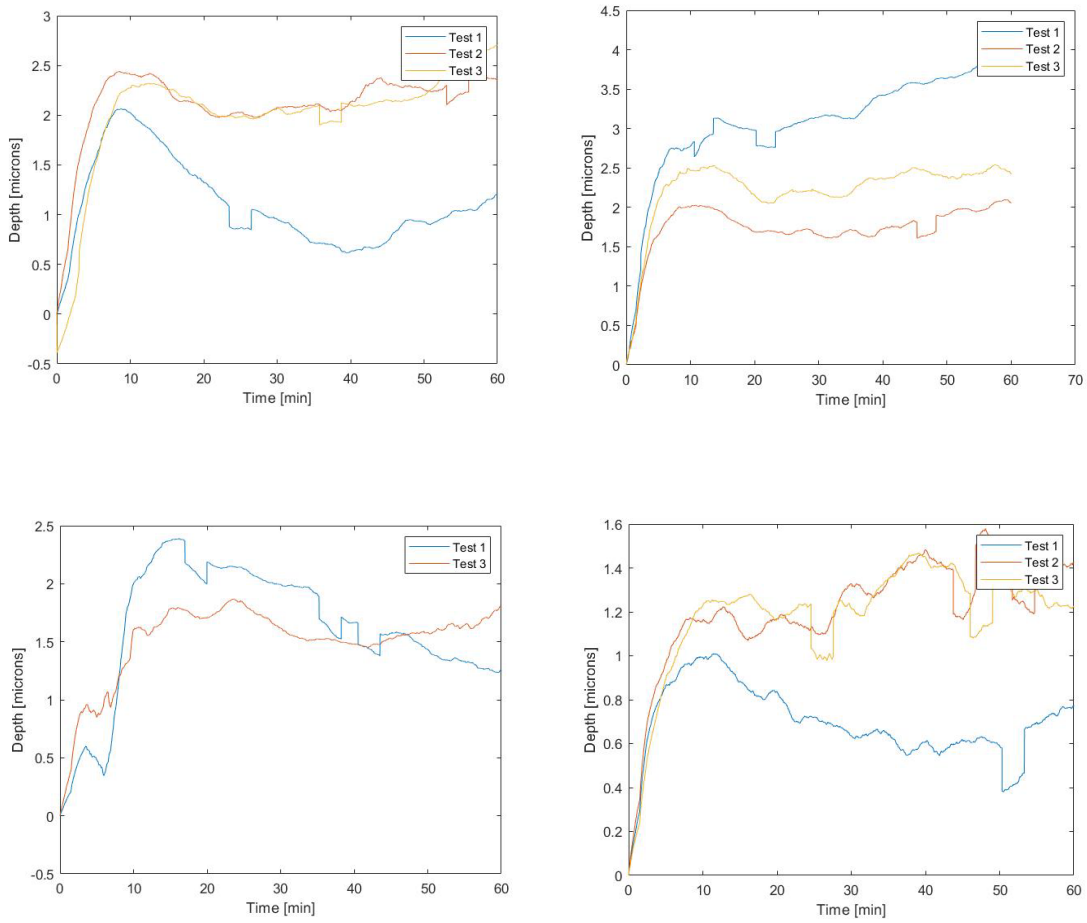

Figure 54. Encoder depth during wear testing. (Clockwise from top left: graded coating 1, graded coating 2, graded coating 4, graded coating 3)

As seen in Figure 54, the depth encoder results varied in depth for each coating, therefore these results must be compared to the results as seen in Figure 52 for the average mass lost during testing. As can be seen from the results in Figure 54, the graded coatings 3 and 4, which contained 30 vol.% of alumina had a lower recorded depth during testing. However, the highest average for recorded depth was from graded coating 2, which does not equate to the greatest average mass loss during testing.

The wear tracks that are created during ball-on-disk dry sliding wear tests are a combination of removing debris from the coating and pushing it along and into the grooves of the wear track as well as completely removing material from the track. For this reason, and to further understand the depth results from the wear testing, optical profilometry was

used to 3-D scan the surface of all wear tracks created during testing. Figure 55 shows an optical scan from graded coating 2 Figure 56 shows an example of the depth measurements taken during the scan, which were then used to find the average depth of each track created. These results were compiled, and an average was taken to determine the total average volume of material lost from each sample. The average volume lost was used in conjunction with the force applied during testing as well as the total distance traveled to calculate the specific wear rate of each coating [44]. Specific wear rates for all four coatings were calculated from the specific wear equation (Equation (2)) [44]; where W_{RS} denotes the specific wear rate, V denotes the volume of material lost, N denotes the applied force, and D denotes the total wear distance. These values, as well as the average depth reading from the optical profilometry results are detailed in Table 14.

$$W_{RS} = \frac{(V)}{(N)(D)} \tag{2}$$

Table 14. Average wear depths and specific wear rates

Graded Coating Number	Average wear track depth (µm)	Specific Wear Rate [(mm^3)/(N)(m)]
1	38.27	0.0047
2	40.28	0.0053
3	31.81	0.0039
4	32.01	0.0039

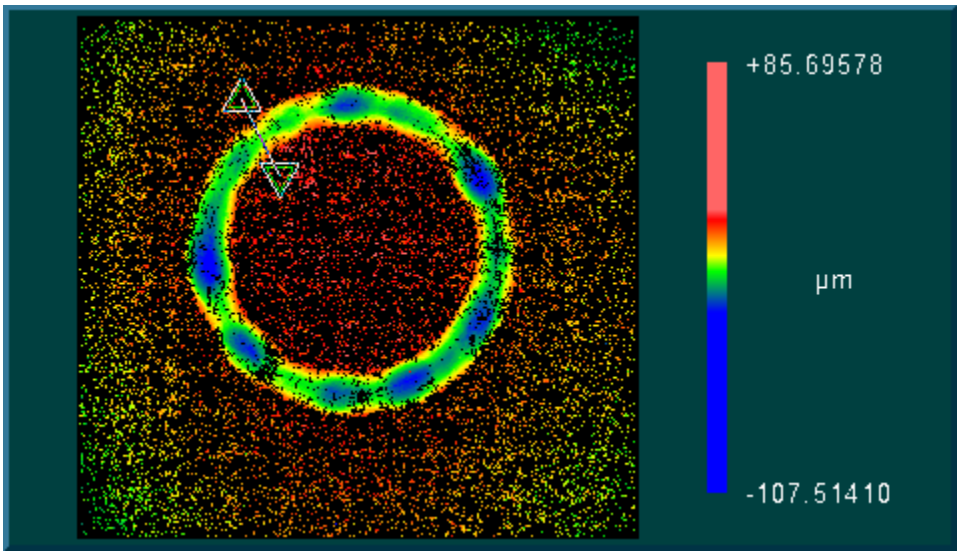

Figure 55. Optical profilometry scan for graded coating 2.

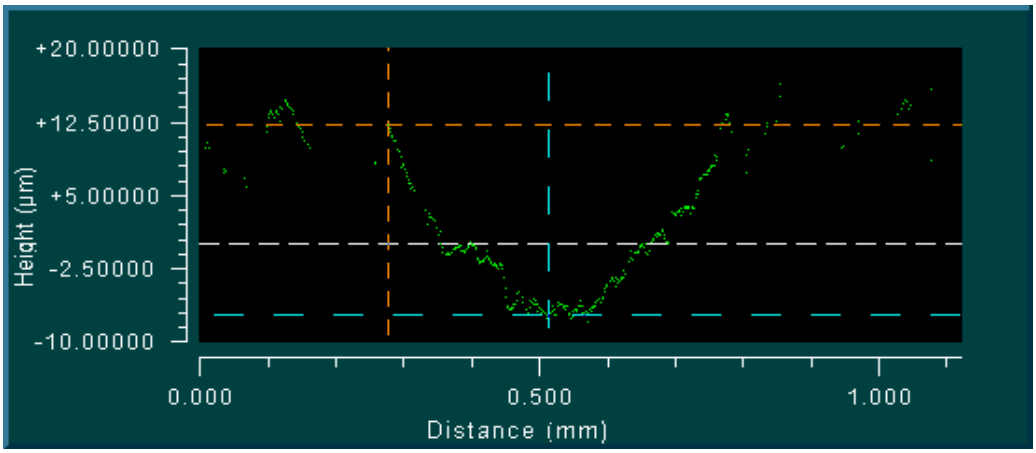

Figure 56. Optical profilometry depth reading for graded coating 4.

The optical profilometry results clearly indicate that the wear tests wore through the entire coating and into the substrate. This is mainly attributed to the thickness of the coating itself, and results from this wear test do not indicate with any certainty that these coatings, with their ceramic reinforcements, enhanced the wear resistant properties of any of the coating compositions. Based on previous literature reviews dealing with alumina used as the reinforcement particle in a cold sprayed Al-MMC, it would seem the results that were obtained during this study do in fact track with previous studies, specifically Fernadez et al. [30]. The results from this study lead to the conclusion that Al-7075

compositions containing 30 vol.% alumina might possibly increase the wear resistance when compared to lower alumina vol.%, as seen from the mass loss and specific wear rate recorded above. However, further testing is required, specifically samples that have a coating thickness large enough to maintain the integrity of the substrate below.

V. CONCLUSION

A. SUMMARY

The primary intent of this study was to compare the effects of compositionally graded, dual-reinforced Al-MMC cold spray coatings reinforced with BNNTs and varying vol.% of alumina. Before this study, there had not been any work on the mechanical properties of graded layers using BNNTs and alumina as composite reinforcements within a cold spray composition. This study specifically looked at the adhesion and wear resistance of the graded cold spray coatings. During the cold spray process, many attempts were made to determine the best operating parameters to achieve a coating that would suit mechanical testing with further analysis through microscopy. However, the thickness of the coating samples did not allow for adequate results during wear resistance testing. Further parameterization of the cold spray process is needed to facilitate better coating depositions and thicknesses when cold spraying with the material utilized in this study. Even with the challenges that were faced, this study provides a solid foundation for the framework needed to further refine compositionally graded cold spray coatings. The adhesion tests conducted in this study provided promising results. It was seen that with the introduction of graded compositional layering during the cold spray process adhesion failure occurred cohesively at the compositional layer interface, leaving a protective layer over the substrate while maintaining adhesion strength near 50 MPa. This study, coupled with the ever-expanding field of cold spray technologies, provides substantial promise to the Department of Defense for tailorable applications of strong, lightweight coatings used to protect surfaces susceptible to degradation while being employed in a myriad of operating environments.

B. RECOMMENDATIONS FOR FUTURE WORKS

The compositions tested in this thesis did not reach a significant deposition thickness which would be required to further evaluate through additional mechanical testing. Refinement of the parameters used during coating application is required to further analyze the effects graded compositional layering may have. Potential parameter changes

would be the substitution of the carrier gas to helium or applying the Al-7075 MMC through a high-pressure cold spray system, thus better ensuring that the sprayed powder particles reach or exceed the critical velocity required for adhesion to the substrate. This would directly affect the Al-7075 particle deformation upon impact to the substrate and would likely result in thicker, denser coatings. Additionally, studies concerning the corrosion resistance of graded compositional coatings could prove valuable to the sustainment of DoD equipment that is exposed to the perils of a marine environment. These studies might include coatings exposed to a salt-fog chamber, polarization resistance tests, and analysis using EDS. Furthermore, the volume percent of various reinforcing ceramics could be altered to determine if specific tailorable properties are achievable.

LIST OF REFERENCES

[1] V. R. Rao, N. Ramanaiah, and M. M. M. Sarcar, "Fabrication and investigation on properties of TiC reinforced Al7075 metal matrix composites," *Appl. Mech. Mater.*, vol. 592–594, pp. 349–353, Jul. 2014, doi: 10.4028/www.scientific.net/AMM.592-594.349.

[2] T. J. Eden and J. Bryant, "Implementation of cold spray technology in navy shipyards and future of cold spray," *NSRP*, Mar. 25, 2020. https://www.nsrp.org/wp-content/uploads/2021/03/ManTech-Project-Implementation-of-Cold-Spray-technology-in-Navy-Shipyards-and-Future-of-Cold-Spray.pdf

[3] D. M. Tauber, "Mechanical properties of nano boron nitride and micro boron carbide reinforced aluminum cold spray coatings," Thesis, MAE, NPS, Monterey, 2023.

[4] J. M. Shockley, S. Descartes, P. Vo, E. Irissou, and R. R. Chromik, "The influence of Al2O3 particle morphology on the coating formation and dry sliding wear behavior of cold sprayed Al–Al2O3 composites," *Surf. Coat. Technol.*, vol. 270, pp. 324–333, May 2015, doi: 10.1016/j.surfcoat.2015.01.057.

[5] R. N. Raoelison *et al.*, "Cold gas dynamic spray technology: A comprehensive review of processing conditions for various technological developments till to date," *Addit. Manuf.*, vol. 19, pp. 134–159, Jan. 2018, doi: 10.1016/j.addma.2017.07.001.

[6] S. Kumar, M. Kumar, and N. Jindal, "Overview of cold spray coatings applications and comparisons: a critical review," *World J. Eng.*, vol. 17, no. 1, pp. 27–51, Jan. 2020, doi: 10.1108/WJE-01-2019-0021.

[7] P. Cavaliere and A. Silvello, "Fatigue behaviour of cold sprayed metals and alloys: critical review," *Surf. Eng.*, vol. 32, no. 9, pp. 631–640, Sep. 2016, doi: 10.1179/1743294415Y.0000000100.

[8] O. C. Ozdemir, C. A. Widener, D. Helfritch, and F. Delfanian, "Estimating the effect of helium and nitrogen mixing on deposition efficiency in cold spray," *J. Therm. Spray Technol.*, vol. 25, no. 4, pp. 660–671, Apr. 2016, doi: 10.1007/s11666-016-0394-8.

[9] R. Osthus, "What is cold spray | VRC metal systems," Apr. 20, 2021. https://vrcmetalsystems.com/what-is-cold-spray/ (accessed Feb. 21, 2023).

[10] H. Assadi, F. Gärtner, T. Stoltenhoff, and H. Kreye, "Bonding mechanism in cold gas spraying," *Acta Mater.*, vol. 51, no. 15, pp. 4379–4394, Sep. 2003, doi: 10.1016/S1359-6454(03)00274-X.

[11] T. Schmidt *et al.*, "From particle acceleration to impact and bonding in cold spraying," *J. Therm. Spray Technol.*, vol. 18, no. 5–6, p. 794, Dec. 2009, doi: 10.1007/s11666-009-9357-7.

[12] S. Buhl, P. Breuninger, and S. Antonyuk, "Optimization of a laval nozzle for energy-efficient cold spraying of microparticles," *Mater. Manuf. Process.*, vol. 33, no. 2, pp. 115–122, Jan. 2018, doi: 10.1080/10426914.2017.1279322.

[13] S. P. Rice, "Enhancing mechanical properties of cold-sprayed aluminum coatings using graphene-nanoplatelet and micro-boron-carbide reinforcements," M. S. Thesis, MAE, NPS, Monterey, 2022.

[14] R. S. Lima, J. Karthikeyan, C. M. Kay, J. Lindemann, and C. C. Berndt, "Microstructural characteristics of cold-sprayed nanostructured WC–Co coatings," *Thin Solid Films*, vol. 416, no. 1–2, pp. 129–135, Sep. 2002, doi: 10.1016/S0040-6090(02)00631-4.

[15] D. A. Rigney, "Sliding wear of metals," *Annu Rev Mater Sci*, vol. 18, no. 1, pp. 141–163, Aug. 1988, doi: 10.1146/annurev.ms.18.080188.001041.

[16] Y. Xiong, W. Zhuang, and M. Zhang, "Effect of the thickness of cold sprayed aluminium alloy coating on the adhesive bond strength with an aluminium alloy substrate," *Surf. Coat. Technol.*, vol. 270, pp. 259–265, May 2015, doi: 10.1016/j.surfcoat.2015.02.048.

[17] H. Assadi *et al.*, "On parameter selection in cold spraying," *J. Therm. Spray Technol.*, vol. 20, no. 6, pp. 1161–1176, Dec. 2011, doi: 10.1007/s11666-011-9662-9.

[18] Y. T. R. Lee, H. Ashrafizadeh, G. Fisher, and A. McDonald, "Effect of type of reinforcing particles on the deposition efficiency and wear resistance of low-pressure cold-sprayed metal matrix composite coatings," *Surf. Coat. Technol.*, vol. 324, pp. 190–200, Sep. 2017, doi: 10.1016/j.surfcoat.2017.05.057.

[19] M. Yandouzi *et al.*, "Microstructure and mechanical properties of B4C reinforced Al-based matrix composite coatings deposited by CGDS and PGDS processes," *Surf. Coat. Technol.*, vol. 205, no. 7, pp. 2234–2246, Dec. 2010, doi: 10.1016/j.surfcoat.2010.08.143.

[20] T. Norrell, G. Ferguson, T. Ansell, T. Saladin, A. Nardi, and A. Nieto, "Synthesis and corrosion behavior of cold sprayed dual nanoparticle reinforced Al coatings," *Surf. Coat. Technol.*, vol. 401, p. 126280, Nov. 2020, doi: 10.1016/j.surfcoat.2020.126280.

[21] E. Irissou, J.-G. Legoux, B. Arsenault, and C. Moreau, "Investigation of Al-Al2O3 cold spray coating formation and properties," *J. Therm. Spray Technol.*, vol. 16, no. 5–6, pp. 661–668, Dec. 2007, doi: 10.1007/s11666-007-9086-8.

[22] P. Nautiyal, C. Rudolf, A. Loganathan, C. Zhang, B. Boesl, and A. Agarwal, "Directionally aligned ultra-long boron nitride nanotube induced strengthening of aluminum-based sandwich composite: Boron Nitride Nanotube Induced Strengthening of Aluminum Composite," *Adv. Eng. Mater.*, vol. 18, no. 10, pp. 1747–1754, Oct. 2016, doi: 10.1002/adem.201600212.

[23] K. K. Pandey *et al.*, "Microstructural and mechanical properties of plasma sprayed boron nitride nanotubes reinforced alumina coating," *Ceram. Int.*, vol. 47, no. 7, pp. 9194–9202, Apr. 2021, doi: 10.1016/j.ceramint.2020.12.045.

[24] N. Yanar, E. Yang, H. Park, M. Son, and H. Choi, "Boron nitride nanotube (BNNT) membranes for energy and environmental applications," *Membranes*, vol. 10, no. 12, p. 430, Dec. 2020, doi: 10.3390/membranes10120430.

[25] N. Kostoglou *et al.*, "Boron nitride nanotubes versus carbon nanotubes: A thermal stability and oxidation behavior study," *Nanomaterials*, vol. 10, no. 12, p. 2435, Dec. 2020, doi: 10.3390/nano10122435.

[26] K. S. Kim *et al.*, "Scalable manufacturing of boron nitride nanotubes and their assemblies: a review," *Semicond. Sci. Technol.*, vol. 32, no. 1, p. 013003, Jan. 2017, doi: 10.1088/0268-1242/32/1/013003.

[27] J. H. Kim, T. V. Pham, J. H. Hwang, C. S. Kim, and M. J. Kim, "Boron nitride nanotubes: synthesis and applications," *Nano Converg.*, vol. 5, no. 1, p. 17, Dec. 2018, doi: 10.1186/s40580-018-0149-y.

[28] N. G. Chopra *et al.*, "Boron nitride nanotubes," *Science*, vol. 269, no. 5226, pp. 966–967, Aug. 1995, doi: 10.1126/science.269.5226.966.

[29] R. Fernandez and B. Jodoin, "Cold spray aluminum–alumina cermet coatings: effect of alumina morphology," *J. Therm. Spray Technol.*, vol. 28, no. 4, pp. 737–755, Apr. 2019, doi: 10.1007/s11666-019-00845-5.

[30] R. Fernandez and B. Jodoin, "Cold spray aluminum–alumina cermet coatings: effect of alumina content," *J. Therm. Spray Technol.*, vol. 27, no. 4, pp. 603–623, Apr. 2018, doi: 10.1007/s11666-018-0702-6.

[31] T. Y. Ansell, T. Hanneman, A. Gonzalez-Perez, C. Park, and A. Nieto, "Effect of high energy ball milling on spherical metallic powder particulates for additive manufacturing," *Part. Sci. Technol.*, vol. 39, no. 8, pp. 981–989, Nov. 2021, doi: 10.1080/02726351.2021.1876192.

[32] P. S. Gilman and J. S. Benjamin, “Mechanical alloying,” *Annu Rev Mater Sci*, vol. 13, no. 1, pp. 279–300, Aug. 1983, doi: 10.1146/annurev.ms.13.080183.001431.

[33] M. L. Trudeau, R. Schulz, D. Dussault, and A. Van Neste, “Structural changes during high-energy ball milling of iron-based amorphous alloys: Is high-energy ball milling equivalent to a thermal process?,” *Phys. Rev. Lett.*, vol. 64, no. 1, pp. 99–102, Jan. 1990, doi: 10.1103/PhysRevLett.64.99.

[34] H. Kaftelen and M. Öveçoğlu, “Microstructural characterization and wear properties of ultra-dispersed nanodiamond (UDD) reinforced Al matrix composites fabricated by ball-milling and sintering,” *J. Compos. Mater.*, vol. 46, no. 13, pp. 1521–1534, Jun. 2012, doi: 10.1177/0021998311421636.

[35] D. J. Woo, F. C. Heer, L. N. Brewer, J. P. Hooper, and S. Osswald, “Synthesis of nanodiamond-reinforced aluminum metal matrix composites using cold-spray deposition,” *Carbon*, vol. 86, pp. 15–25, May 2015, doi: 10.1016/j.carbon.2015.01.010.

[36] W. Huo, J. Hu, H. Cao, Y. Du, W. Zhang, and Y. Zhang, “Simultaneously enhanced mechanical strength and inter-granular corrosion resistance in high strength 7075 Al alloy,” *J. Alloys Compd.*, vol. 781, pp. 680–688, Apr. 2019, doi: 10.1016/j.jallcom.2018.12.024.

[37] A. E. Paladino and W. D. Kingery, “Aluminum ion diffusion in aluminum oxide,” *J. Chem. Phys.*, vol. 37, no. 5, pp. 957–962, Sep. 1962, doi: 10.1063/1.1733252.

[38] S. Abiodun, R. Krishnamoorti, and A. K. Bhowmick, “Polytetrafluoroethylene nanocomposites with engineered boron nitride nanobarbs for thermally conductive and electrically insulating microelectronics and microwave devices,” *ACS Appl. Nano Mater.*, vol. 6, no. 5, pp. 3781–3796, Mar. 2023, doi: 10.1021/acsanm.2c05437.

[39] Y. Qiu and Z. Zhang, “Effects of internal electromagnetic stirring on the microstructure refinement and composition homogenization of large-scale 7075 aluminum alloy billet,” *JOM*, vol. 73, no. 12, pp. 3812–3818, Dec. 2021, doi: 10.1007/s11837-021-04875-9.

[40] S. Singh, R. K. S. Raman, C. C. Berndt, and H. Singh, “Influence of cold spray parameters on bonding mechanisms: A Review,” *Metals*, vol. 11, no. 12, p. 2016, Dec. 2021, doi: 10.3390/met11122016.

[41] G. F. Vander Voort, "Metallography, principles and practice," Materials Park, OH: ASM International, 1999.

[42] “EP15ND-2 Product Information | MasterBond.com.” https://www.masterbond.com/tds/ep15nd-2 (accessed Mar. 24, 2023).

[43] The National Shipbuilding Research Program Surface Preparation and Coatings Panel. "Application of polysiloxane topcoats during shipbuilding." 2015 [Online]. Available: https://www.nsrp.org/wp-content/uploads/2015/09/Deliverable-2014-430-Polysiloxane_vs_Silicone_Final_Report-Bath_Iron_Works.pdf

[44] A. Güneş *et al.*, "Towards analysis and optimization for contact zone temperature changes and specific wear rate of metal matrix composite materials produced from recycled waste," *Materials*, vol. 14, no. 18, p. 5145, Sep. 2021, doi: 10.3390/ma14185145.

THIS PAGE INTENTIONALLY LEFT BLANK

INITIAL DISTRIBUTION LIST

1. Defense Technical Information Center
   Ft. Belvoir, Virginia

2. Dudley Knox Library
   Naval Postgraduate School
   Monterey, California